SCIENCE CHINA
Chemistry

•REVIEWS•

July 2018 Vol.61 No.7: 765–786
https://doi.org/10.1007/s11426-018-9270-y

2D graphdiyne materials: challenges and opportunities in energy field

Yurui Xue[1], Yuliang Li[1*], Jin Zhang[2], Zhongfan Liu[2] & Yuliang Zhao[3]

[1]*CAS Key Laboratory of Organic Solids, Institute of Chemistry, Chinese Academy of Sciences, Beijing 100190, China;*
[2]*Center for Nanochemistry, College of Chemistry and Molecular Engineering, Peking University, Beijing 100871, China;*
[3]*National Center for Nanoscience and Technology, Chinese Academy of Sciences, Beijing 100190, China*

Received March 26, 2018; accepted April 23, 2018; published online May 31, 2018

Graphdiyne (GDY), a novel two-dimensional (2D) carbon allotrope featuring one-atom-thick planar layers of sp and sp^2 co-hybridized carbon network, is a rapidly rising star on the horizon of materials science. Because of its unparalleled structural, electronic, chemical and physical properties, it has been receiving unprecedented increases from fundamental studies to practical applications, particularly the field of energetic materials. In this review, we aim at providing an up-to-date comprehensive overview on the state-of-the-art research into GDY, from theoretical studies to the key achievements in the development of new GDY-based energetic materials for energy storage and conversion. By reviewing the state-of-the-art achievements, we aim to address the benefits and issues of GDY-based materials, as well as highlighting the existing key challenges and future opportunities in this exciting field.

graphdiyne, semiconductor, two-dimensional carbon materials, nanostructure

Citation: Xue Y, Li Y, Zhang J, Liu Z, Zhao Y. 2D graphdiyne materials: challenges and opportunities in energy field. *Sci China Chem*, 2018, 61: 765–786, https://doi.org/10.1007/s11426-018-9270-y

1 Introduction

Carbon-rich materials are at the leading edge of the rapid development of nanotechnologies, offering large amounts of promising alternatives to precious materials used in sustainable energetic applications due to their excellent mechanical, electronic, optical and electrochemical properties. Generally, carbon atoms are present in one of the sp, sp^2, or sp^3 hybridization states which are associated with linear, trigonal, and tetrahedral geometries, respectively, and can be combined together in various strategy to create new allotropes with potentially interesting physiochemical properties (Figure 1) [1–5]. Over the last few decades, the entire realm of carbon materials has evolved at an incredible pace from the discovery of fullerenes [6] (zero-dimensional, 0D, C60, 1985) to carbon nanotubes [7] (one-dimensional, 1D, CNT, 1991), and graphene [8] (2D, 2004). The impetus for these revolutionary changes might emanate from their unique properties and the increasing use of carbon materials in our daily lives.

While previous work has focused on graphitic carbons, we believe that other types of pure carbon materials are feasible using different accessible hybridization states of carbon. A typical example of such carbon materials is graphyne (GY), which is first proposed by Baughman *et al.* [9] in 1987, one year later after the proposal of "graphene" [10], is an allotrope of carbon and can be regarded as a lattice of benzene rings connected by acetylenic linkages. GY is the generic name for the family of 2D carbon nanostructures similar to graphene, but with the introduction of acetylenic linkages (sp-hybridized carbon) between repeating benzene rings (sp^2-hybridized carbon). The geometries and percentages of

*Corresponding author (email: ylli@iccas.ac.cn)

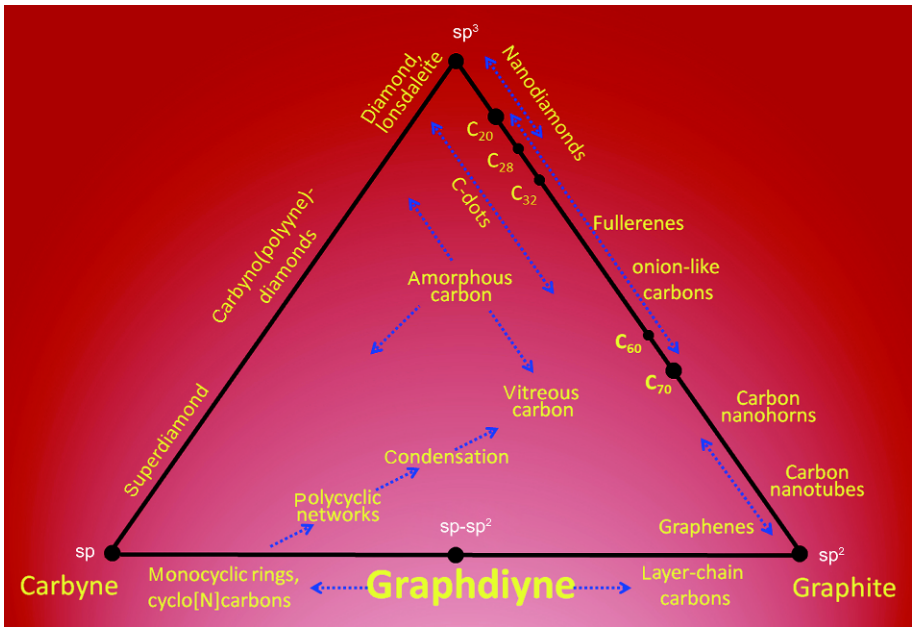

Figure 1 A phase diagram showing materials consisting of carbon in a single hybridization state at the vertices, materials containing mixtures of two hybridization states along the edges, and materials with all three hybridization states within the triangle (color online).

these linkages are used to define each GY subtype. The presence of acetylenic groups in GY generates a rich variety of optical and electronic properties that are quite different from those of conventional carbon materials. GY and a series of its similar atomic structures (e.g., graphdiyne (GDY), graphtriyne (GY-3), and graphtetrayne (GY-4)) lie at the frontier of theoretical and experimental nanomaterial science. The linear carbon chain between carbon hexagons is shown to be more stable to be composed of acetylenic linkages (–C≡C–) than cumulenic linkages (=C=C=) [11].

Among various GY structures, GDY (GY with diacetylenic bonds) [12], featuring one-atom-thick planar layers of sp and sp^2 co-hybridized carbon atoms arranged in crystal lattice, is theoretically predicted to be the most "synthetically approachable" and stable allotropes with atomic thickness [12–15]. The planar carbon network (sp- and sp^2-hybridized) endows GDY with high π-conjunction, uniformly distributed pores, and tunable electronic properties, which can make the new 2D carbon materials promising for versatile applications [2,16]. Moreover, carbon networks with delocalized π systems are of particular relevance since their properties can be tuned along with changes in their electronic and chemical configurations. GDY has been initially targeted by Haley *et al.* [12] in 1997. From then on, great efforts have been devoted to the synthesis of monomeric and oligomeric substructures toward constructing GDY [12–15,17]. Until very recently in 2010, Li and co-workers [2,5,18] successfully synthesized GDY films with high-quality on the surface of Cu foil via cross-coupling reaction using hexaethynylbenzene precursors for the first time. The as-prepared GDY exhibits excellent semiconducting properties similar to silicon, which is a vital candidate to apply in the fields of electronics, semiconductors and materials [19]. GDY is proposed to have intriguing high third-order nonlinear optical susceptibility, high fluorescence efficiency, extreme in-plane hardness, high thermal resistance, conductivity or superconductivity, and through-sheet transport of ions. Theoretical studies also showed that the transition metal-adsorbed GDY (TM-GDY) could be more stable than corresponding TM-adsorbed graphene [20]. Based on these, GDY has been attracting increased attention from both fundamental studies and practical applications. The series of events described above clearly demonstrate that GDY is a fascinating carbon-rich material and is able to form various morphologies at the nanoscale, possessing different physicochemical properties, some of them yet unknown. It is believed that GDY with different dimensions from 0D to 1D and 2D can be superior to "conventional" carbon materials, including fullerenes, carbon nanotubes, and graphene, respectively, in various potential applications and meet the increasing demand for carbon-based nanomaterial.

This review highlights the main properties of GDY as a novel 2D carbon allotrope for the fabrication of functional nanostructures and their exciting applications in energetic fields. We first summarize the fundamental theoretical predictions of the potential properties of GDY and GDY-based nanomaterials. The latest advances in tailoring their electronic, chemical, and mechanical properties based on the morphological engineering will then be discussed. In addition, we discuss the state-of-the-art experimental attempts to synthesize and apply novel GDY-based materials in the areas of electronics, optics, and catalysis. Finally, this perspective

review highlights the existing key challenges and future opportunities in this exciting field.

2 Theoretical studies

2.1 Geometric analysis

GY, predicted by Baughman and co-workers [9] in 1987, one year later after the proposal of "graphene" [10], is an allotrope of carbon and can be regarded as a lattice of benzene rings connected by acetylenic linkages. The name "GY" results from its structure, namely, the layers can be constructed by replacing one-third of the carbon-carbon bonds in graphite with acetylenic linkages (–C≡C–), resulting a one-atom-thick sheet of sp and sp^2 co-hybridized carbon network. Depending on the content of acetylene groups, GY has a mixed hybridization (sp^n, where $1<n<2$), and thus differs from graphene (considered pure sp^2) and diamond (pure sp^3) (Figure 2). The presence of acetylenic linkage introduces nonzero band gap in GY sheet [11,18,19], which is absent in pristine graphene. Potential modification of the number of acetylene groups may enable a rich variety of accessible optical and electronic properties that are quite different from those of graphene or carbon nanotubes [2,11,21–33].

For GYs, the single bonds have contracted and the aromatic bonds extended compared to typical values (from approximately 1.54 and 1.40 Å, respectively). Qualitatively, the presence of the acetylene groups have been shown to reduce the aromatic character of the benzene ring, where the length of the shared bond between the acetylene groups and the benzene ring is elongated presumably due to weak conjugation between the two alkyne units and the benzene ring [21,34]. The average bond lengths were commonly used to quantify their lattice spacing. Previous results [11,21,35] showed the similar homogeneous increases in the lattice spacing of extended GYs, implying that the addition of extended acetylene linkages would not result in significant structural changes. Moreover, the averaged carbon-carbon bond lengths for single networks of hexagonal GY and GDY are not uniform, suggesting different bonding types: =C=C=, –C≡C–, =C–C≡, and ≡C–C≡. This diversity of carbon-carbon bonds will result in greater structural flexibility for GYs as compared with graphene, which should be very beneficial for the fabrication of curved structures such as nanotubes. GDY nanoribbons (GDYNRs), which are important in nanoelectronic engineering, have been examined [19]. There are two major ways to cut the sheet into ribbons, such as cutting GDY along the direction of the nearest neighboring hexagons resulting in divan-like edged GDYNR (DGDYNR) or along the next nearest neighboring hexagons forming zigzag-like edged GDYNR (ZGDYNR). All GDYNRs are predicted to be semiconductor, in which the DGDYNR with three carbon hexagons in edge shows the smallest band gap of ~0.8 eV at the Γ-point.

2.2 Mechanical properties

Mechanical properties are another attractive features of GY. Cranford *et al.* [34] characterized the mechanical properties of single-atomic-layer of GY sheets by full atomistic first-principles-based ReaxFF molecular dynamics. The energy minimized GY sheet showed near-constant bond length values of 1.19, 1.48, and 1.49 Å for triple, single, and aromatic bonds, respectively. The weak interactions (i.e., primarily van der Waals interactions) between two GY surfaces were characterized. In this process, two copied GY sheets are simulated together and moved into close proximity to one another while calculating the potential energy over the range of distances. The equilibrium distance (at energy minima) between two GY layers was determined to be 3.20 Å, which is smaller than that of graphene/graphite (3.35 Å) due to the more sparse arrangement of carbon atoms within the GY sheet, resulting in a weaker surface energy landscape and thus closer equilibrium contact between layers. Moreover, the sparser layout of in-plane carbon atoms per sheet of GY resulted in a smaller adhesion energy (223.5 mJ/m^2) than that

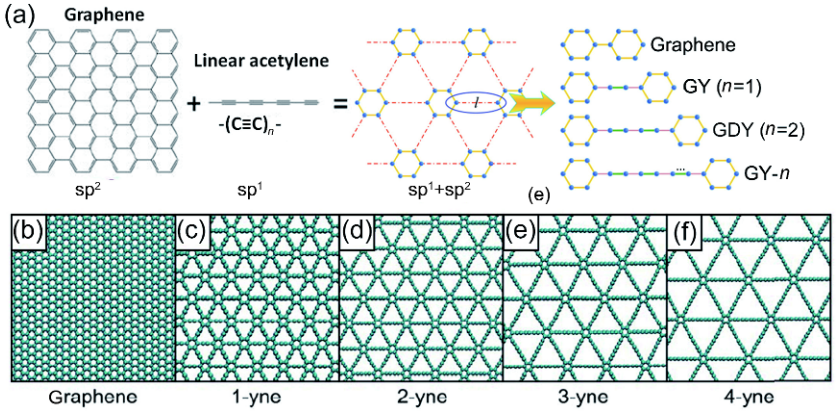

Figure 2 (a) Schematic of graphene to graphyne-linking aromatic groups by linear acetylene. Constructed full atomistic molecular models for grapheme (b), GY (c), GDY (d), GY-3 (e), and GY-4 (f) [21] (color online).

of graphene (260−345 mJ/cm^2). Since the first synthesis of GDY was reported by Li's group [18], the potential uses of GDY in future have attracted much attention. Understanding its contact with substrate surface (such as copper foil) is of great significance for its applications. The interfacial structural, mechanical and electronic properties of the contact between GDY and Cu(111) surface have recently been characterized through first principles calculations by Yang *et al.* (Figure 3) [36]. With interface distance decreasing, charges are transferred from the copper surface to the upper layer GDY, and different bond interactions occur between surface Cu atoms and GDY, which make the contact between GDY and copper surface more tightly and provide a bridge for charge transfer at the interface.

Unlike graphene, the fracture strain and stress of GY is predicted to depend strongly on the direction of the applied strain and the alignment with carbon triple-bond linkages, ranging from 48.2 to 107.5 GPa with ultimate strains of 8.2%–13.2%. The inter-sheet adhesion and out-of-plane bending stiffnesses are comparable to graphene, despite the density of GY being only one-half of that of graphene. Moreover, the sparser carbon arrangement in GY combined

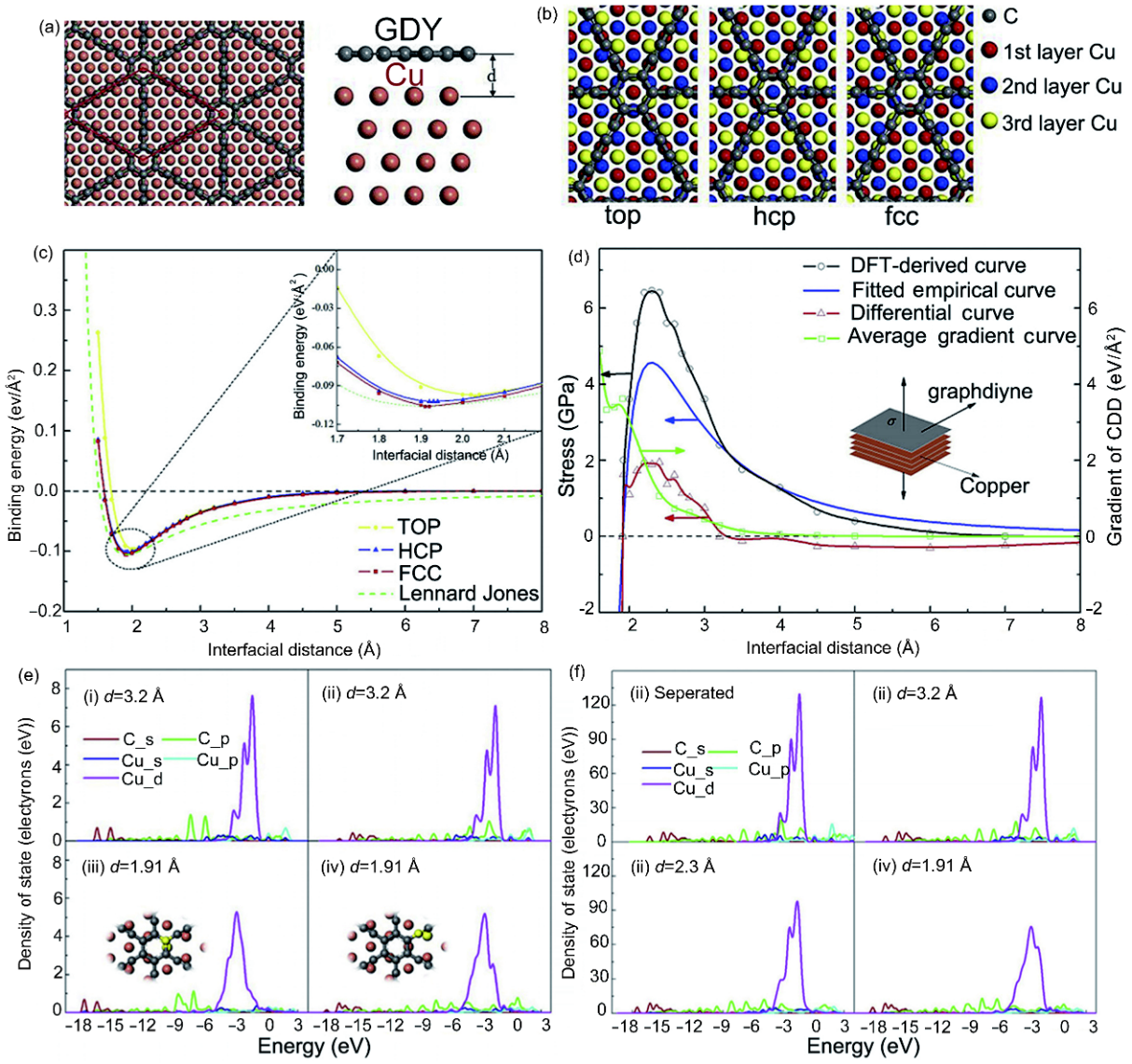

Figure 3 (a) Structure of the interface between monolayer GDY and Cu(111) surface. (a) Top view and side view of the unit supercell, *d* is the interface distance. (b) Top views of top, hcp and fcc configurations, respectively. (c) is the relationship between binding energies and interface distance for different stacking configurations. The dashed line is the *L-J* fitting curve based on the fcc curve. (d) The change of bonding strength and gradient of charge density difference (CDD) during the interface peeling process. The curve in red is the difference between DFT-derived and fitted empirical curves. (e) The projected spin densities of states (PDOSs) of specific C and Cu atoms at different interface distances. (i) and (iii) are PDOSs for the sp^2 C atom and the Cu atom below at interface distances of 3.2 and 1.91 Å respectively; (ii) and (iv) are PDOSs for the sp C atom and the Cu atom below at interface distances of 3.2 and 1.91 Å respectively. (f) PDOSs of graphdiyne and surface copper atoms at different interface distances. (i) is the PDOS of separated graphdiyne and surface copper atoms, (ii), (iii) and (iv) are PDOSs of the two components at interface distances of 3.2, 2.3 and 1.91 Å, respectively [36] (color online).

with the directional dependence on the acetylenic linker results in internal stiffening dependent on the direction of applied loading, leading to a nonlinear stress-strain behavior. Cranford *et al.* [21] found that the introduction of acetylene links introduces an effective penalty in terms of stability, elastic modulus (i.e., stiffness), and failure strength, which can be predicted as a function of acetylene repeats, or, equivalently, lattice spacing. The mechanical properties of experimental accessible GDY were quantified, with a modulus on the order of 470 to 580 GPa and a ultimate strength on the order of 36 to 46 GPa (direction dependent).

The relationship between in-plane stiffness and number of acetylenic linkages follows a simple scaling law. As shown in Figure 4, the in-plane stiffness of GY-*n* decreases with increasing acetylenic linkage number, and is in excellent agreement with the existing numerical results [22,38–40]. For example, Yang *et al.* [38] showed that the in-plane stiffness of graphyne-*n* degrades from 150 to 50 N/m (~67% reduction) with the increasing acetylenic linkage number from one to five. Yue *et al.* [39] showed that the in-plane stiffness C of GY (166 N/m), GDY (123 N/m), GY-3 (102 N/m), and GY-4 (88 N/m) decrease with the increasing number of –C≡C–, whereas Poisson's ratio (v) are 0.416, 0.446, 0.436, and 0.432, respectively, revealing only a small variation. Hou *et al.* [37] found that, as the number of acetylenic linkages increases from one to 10, the shear stiffness decreases from 75.6 to 12.3 N/m, whereas the Poisson's ratio increases from 0.19 to 0.30 (Figure 4). The reduction in the in-plane stiffness (from about 180 to 40 N/m) and shear stiffness is attributed to the smaller atom/bond density. But a longer acetylenic chain which has a lower bending resistance will lead to a larger lateral deflection and thus to a higher Poisson's ratio. Kang *et al.* [40] obtained similar v of 0.417 and an in-plane stiffness from first-principles calculations, which are performed using frozen-core projector-augmented wave method as implemented in the Vienna *ab initio* simulation package (VASP) [41]. The work of Zhang *et al.* [42] indicated that the presence of the acetylenic linkages in the GY structures influenced their Young's moduli, fracture strains, and fracture stresses. It is also found that the fracture stress and strain of graphene and GYs in the zigzag (x) direction are higher than those in the armchair (y) direction.

The formation energy per atom can generally be used to assess the relative stability of each GY/GDY. It was firstly predicted that GY would have a high temperature-stability because of the reasonably low solid-state formation energy (12.4 kcal/mol carbon) and the fact that transformation of GY to graphite requires at least one rupture of a covalent bond for every six carbons in GY [9]. The calculated Gibbs free energy for 2D GDY layer and 1D GDY nanoribbons (with respect to graphene) are 0.803 eV per atom and in the range of 0.520–0.775 eV per atom, respectively; the corresponding values for diamond, graphite, (6,6)-nanotubes, C_{60}, and carbyne are approximately −0.022, −0.008, 0.114, 0.364, and 1.037 eV per atom, respectively [35]. Therefore, the stability of GY/GDY decreases as a result of the presence of acetylenic/diacetylenic linkers. This was also confirmed by another simulation based on density functional theory tight-binding (DFT-TB) method for systematically studying the

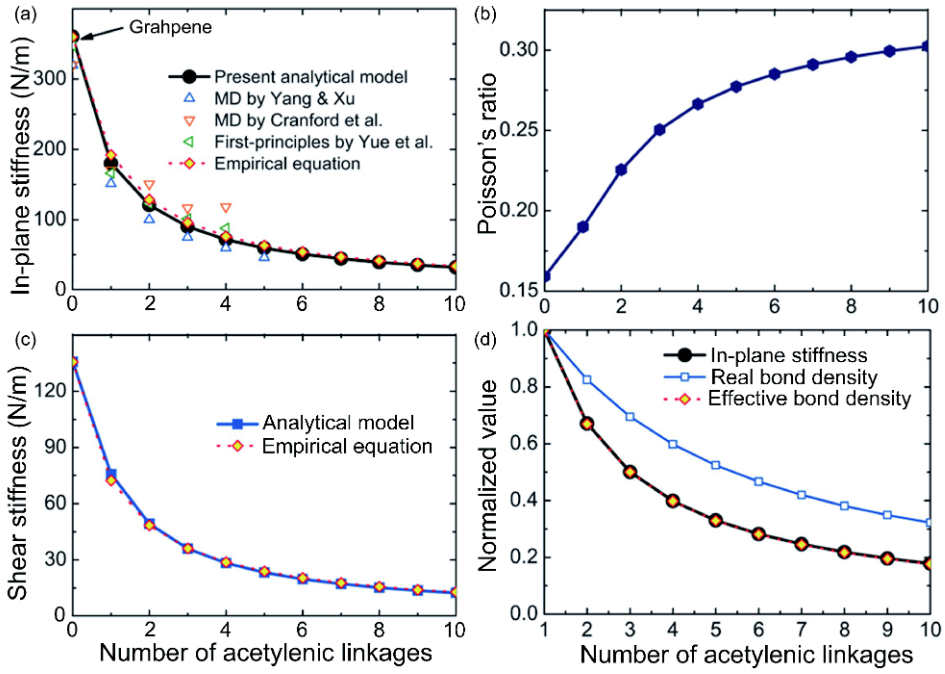

Figure 4 (a) In-plane stiffness, (b) shear stiffness, and (c) Poisson's ratio of graphyne-*n* as functions of the number of acetylenic linkages. (d) Dependence of the normalized in-plane stiffness, real bond density, and effective bond density on the number of acetylenic linkages [37] (color online).

stability and structural properties of series of (sp^1+sp^2)-like 2D carbon networks (such as GY and GDY), where the difference in total energy between the allotrope ($E_{n\text{-yne}}$) and pristine graphene ($E_{graphene}$) was defined as d_E (per carbon atom). Using the fraction of sp^1 and sp^2 carbons, the energies of GYs can be predicted well in terms of the number of acetylene linkages (n) or the hybridization (h) [21]. The introduction of acetylene links leads to an effective penalty in terms of stability. That is, the stability decreases upon increasing the ratio of sp- to sp^2-hybridized carbon atoms.

2.3 Electronic properties

Particular interests have been devoted to electronic properties, motivating previous theoretical, experimental and quantum-scale studies. The excitement surrounding GY is predominantly related to its potential for never-before-seen electronic transport properties. As have been demonstrated by multi-scale computations, unlike graphene (zero band gap), GY and GDY have natural band gap (inherent semiconducting characteristics), and simultaneously possess high electrical conductivity. Variations of the strain, ribbon width, nanotube diameter, edge morphology, and functionalization should open up new and effective ways of tailoring their electronic, chemical, mechanical, and magnetic properties.

2.3.1 Strain effects

In a strain free state, the band gaps were calculated to range from 0.46 to 1.22 eV, depending on the employed methods and exchange-correlation functional [2,9,11,20,21,44–46]. For example, Lu *et al.* [43] obtained a value for the band gap of a GDY monolayer of 1.10 eV using the GW many-body theory. Jiao *et al.* [44] predicted that the band gap of GDY to be 1.22 eV, which is comparable to that of silicon (1.11 eV). He *et al.* [20] indicated that the pristine GDY and GY are direct band gap semiconductors with a band gap of 0.49 and 0.48 eV, respectively, and both their valence band maximum (VBM) and conduction band minimum (CBM) locate at the Γ point. These results bind the range of possible band gaps, limiting it to nonzero values, which presents outstanding advantages over graphene for electronic applications.

Under external strain, the band gaps of the GY family were demonstrated to be tunable by using first principle calculations [38,40,45–47]. The work of Pei [45] found that the band gap of GDY monotonously increases with increasing strain value, which originates from the decreased orbital overlap between C atoms when strain increases. Yue *et al.* [39] showed that the band gaps of GY, GDY, GY-3 and GY-4 decrease under uniaxial tensile, compressive, and homogeneous compressive strains and increase with homogeneous tensile strain. The relation between in-plane stiffness and number of acetylenic linkages can be characterized by a simple scaling law. GDY and GY-4 maintain the direct gap at Γ point under strains, while the band gaps of GY and GY-3 are direct and located at either M or S point depending on the types of applied tensile strains. The variations in their band structures are attributed to the shift of energy states near the Fermi level under strains. Cui *et al.* [47] found that the band gap of GDY increases from 0.47 to 1.39 eV with increasing the biaxial tensile strain, while the band gap decreases from 0.47 eV to nearly zero with increasing the uniaxial tensile strain, and Dirac cone-like electronic structures are observed.

2.3.2 Structural effects

Understanding the structure-electronic relationships can lead to new "design rules" for fabricating benign, high-performance nanomaterials. Zheng *et al.* [48] reported the first systematic *ab initio* investigation on modulation of the electronic structures of bilayer and trilayer GDY under an external electric field (Figure 5). In the most-stable bilayer and trilayer GDYs, the hexagonal carbon rings are stacked in a Bernal manner (AB- and ABA-style configurations, respectively). All of these relatively stable structures are semiconductor: bilayer GDYs with the highest and second-highest stability possess band gaps of 0.35 and 0.14 eV, respectively; trilayer GDYs with stable stacking configurations have band gaps of 0.18–0.33 eV. However, this study only reported the effect of external filed strength on the band gaps of all semiconducting bilayer and trilayer GDYs, decreasing with increasing external field strength, irrespective of the stacking style. Recently, Luo *et al.* [49] studied the structural and electronic properties of bulk GDY and found that, at the HSE06 level, the AA configuration is a metal, whereas the AB-1, AB-2, and AB-3 configurations are semiconductors with band gaps of 0.05, 0.74, and 0.35 eV, respectively. We demonstrate that the electronic properties and the low-energy optical absorption spectra strongly depend on the stacking, and the vdW correction is essential for computing the binding energy and low-energy optical spectra. Based on a first-principles investigation of bilayer α-GY, Leenaerts *et al.* [50] showed that the electronic band structure of bilayer α-GY is qualitatively different from its monolayer form and depends crucially on the stacking mode of the two layers. Two stable stacking modes are found: a configuration with a gapless parabolic band structure (like AB-stacked bilayer graphene) and another one which exhibits a doubled Dirac-cone spectrum and a band structure around the Fermi-level exhibiting a linear dispersion that can be tuned by an electric field with a gap opening rate of 0.3 eV/Å.

Different from the graphene nanoribbons, the GDY and GY nanoribbons are all semiconductors with suitable band gaps [19,32,35], which is essential for nanodevice design and application. Quantitatively, the band gaps of both GDY and GY decrease monotonically as the widths increase [32]. It is also found that the band gap is at the Γ point for all GDY

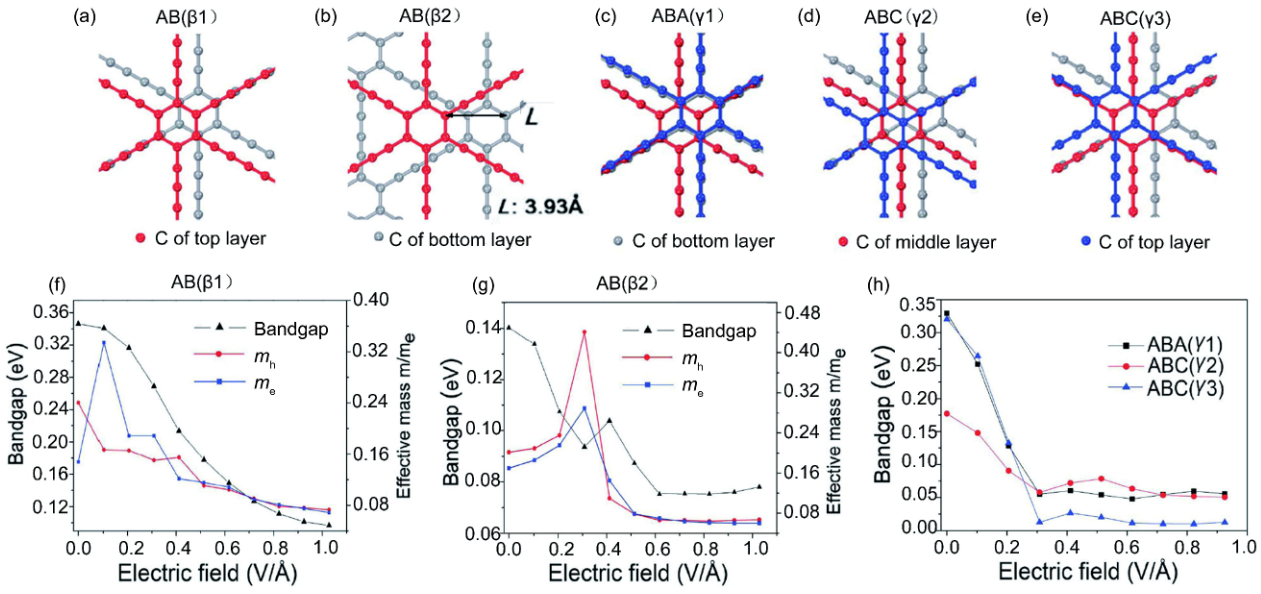

Figure 5 Optimized configurations of (a, b) bilayer and (c–e) trilayer GDY from top view. Band gap (by the left scale) and effective mass of carriers (m_e and m_h, by the right scale) of AB(β1) (f) and AB(β2) (g) configuration of bilayer graphdiyne as a function of perpendicular electrical field strength. Filled squares and circles indicate the calculated m^*_e and m^*_h. (h) Band gaps of ABA(γ1), ABC(γ2), and ABC(γ3) trilayer configurations versus perpendicular electrical field strength [48] (color online).

ribbons and it is at the X point for all GY ribbons. This property is good for tuning of the energy band gap, as in a certain range of the ribbon width, the energy gap remains constant and in reality the edge cannot be as neat as that in a theoretic model. Interestingly, GY nanotubes (GNT) with even richer variation in electronic properties than that of ordinary single wall carbon nanotubes were predicted by Coluci *et al.* [33]. According to their calculation results, the band gap in γ-GNT is independent of the nanotube diameter and chirality. However, further studies conducted by Wang *et al.* [51] and Bhattacharya *et al.* [52], respectively, suggested that the band gap of γ-GNT shows a damped oscillation with the tube diameter increased. According to Bhattacharya *et al.* [52], the band gaps are 0.68 and 1.08 eV for pristine (2,2) and (2,0) GNTs, respectively, and occur at the X point in the Brillouin zone. Recently, By using *ab initio* density functional theory calculations using the SIESTA code, Shohany *et al.* [53] found that the band gaps of both zigzag and armchair GDY nanotubes (ZGDNTs and AGDNTs, respectively) are clearly diameter dependent which decrease by increasing the diameter of the nanotube. Moreover, the AGDNTs have larger band gap and smaller diameter in comparison with ZGDNTs. Zhu *et al.* [54] found that the GDY nanowire (GDYNW) can be classified as a semiconductor with a band gap of 1.762 eV using the PBE method (2.605 eV with HSE06), which is similar to the 1.60 eV value obtained from previous DFT calculations by Cirera *et al.* [55] When an electric field is applied in a direction perpendicular to the wire axis and parallel to the plane of the extended GDYNW, the nanowire still exhibits semiconducting properties, with band gaps ranging from 1.762–2.000 eV. The relationship of the band gaps and the field strength was found to be E_g=0.024E^2+1.760, which would be useful for accurately controlling the band gap of the 1D extended GDYNW. Interestingly, the electronic properties of chemically functionalized (OH, NH_2, CH_3, F, CN, NO_2, and COOH at the polyphenylene edges) 1D GDYNW are still semiconductors despite the fact that the band gaps are somewhat smaller than those of pristine GDYNW; the hole mobility of the extended graphdiyne nanowires with NO_2 and COOH groups is rather low and close to zero because of their rather flat HO bands.

Very recently, the electronic and vibrational properties of the single planar chains of GY and GDY are calculated as a function of the chain length [56]. Both GY and GDY are predicted to be semi-conducting having a non-zero band gap at the zone center (1.0 eV for single GY chains and 0.73 eV for single GDY chains, respectively). The band gap was predicted to be approximately decreased as the length of the chain increased, whereas in the case of the wider sheets the band gap was predicted to be approximately independent of the sheet length.

2.3.3 *Heteroatom doping*

Doping is another effective approach to modulate the electronic properties of GDY/GY. For example, GY with adsorption of Ca represents spin-polarized electronic property with a small localized magnetic moment (~0.25 μB) and shows an excellent properties for hydrogen storage because of its high capacity of hydrogen storage and effective pre-

vention for the formation of Ca cluster [57]. He *et al.* [20] found that the adsorption of transition-metal (TM) atom not only efficiently modulates the electronic structures of GDY/GY system, but also introduces excellent magnetic properties, such as spin-polarized half-semiconductor, which originated from the charge-transfer between TM adatom and GDY/GY as well as the electron redistribution of the TM intra-atomic s, p, and d orbitals. More interestingly, Nickel adsorbed GDY/GY narrows the band gap in comparison with that of pristine GDY/GY. While the doping of boron (B) and nitrogen (N) at different sites of GDY can increase the band gap (the order: pristine system<B/N at chain<B/N at ring<B/N sheet) [52]. This should be due to the fact that the doping of boron (B) and nitrogen (N) inserts some impurity states into the conduction band (CB) and valence band (VB), respectively, near the Fermi level. Recently, Bu *et al.* [58] revealed that with the increase of BN component the band gap of GDY would increase first gradually and then abruptly due to the transition between the two substitution motifs. The direct-band gap feature is intact in these BN-doped graphdiyne regardless the doping rate. Mohajeri *et al.* [59] found that, for GY and GDY, the energy gap can be tuned over a range ~1.0 eV by varying the type (N and NS) and the concentration of dopants. Besides, the GY/GDY energy gap can also be tuned over a wide range of ~1.20 eV through the edge functionalization by correct number of CO group. For both GY and GDY flakes, increasing number of CO and COOH groups would cause a general energy gap reduction; however, a sudden increase in energy gap appears for the flakes with three functional groups, which may be ascribed to the asymmetry in the functionalization of opposed edges.

2.4 Optical properties

The optical properties of carbon nanomaterials has become a major topic of research. A systematic approach to tuning the optical responses of nanomaterials is required for diverse applications, such as optoelectronics, light energy conversion, UV light protection and artificial photosynthesis. The optical property of GY is found to be strongly anisotropic [40], such as, the optical adsorption is significant for in-plane polarization in the low-energy region, but neglectable for out of plane polarization. Luo *et al.* [49] found that the interlayer van der Waals force red shifts the optical absorption peaks of bulk GDY relative to those of the monolayer, and spectra of different stacking display notable differences in the energy range below 1 eV. BN doping could also significantly altered inherent optical properties of both GNTs [52] and GY derivative layers. Compared with their parent two-dimensional structure, BN-substituted analogs exhibit distinct characteristics. They found that the optical band gap is tuned from infrared to UV via visible region depending on the BN substitution sites. For GNTs, the presence of B/N sweeps the first absorption peak of the ε_2 spectra towards the UV region of the electromagnetic spectrum in the order pristine GNT<GNT with B/N at the chain position<GNT with B/N at the ring position<BNGNT; while for GY and derivative layers, all the systems exhibit a strong absorption peak in quite wide UV-region for perpendicular polarization and provide the evidence of strong UV absorption. Additionally, in the presence of NS, the optical energy gap of pristine GY/GDY can be tuned from the visible to the infrared region of the electromagnetic spectra depending on the doping level [59]. The optical energy gaps lie in the visible region for the pristine GY/GDY and in the infrared region for the N-doped and *N*,*S*-codoped GY/GDY. This nature makes the graphyne family and their BN analogues tunable toward their usage in UV light protection.

3 Design and synthesis of GDY-related nanostructures

Since the first experimental synthesis of the GDY in 2010 [18], a major focus of research has been concentrated on the development of new synthetic methods enabling the effective achievement of various morphologies of GDY, e.g., GDY nanotubes [60], GDY nanowires [61,62], and GDY stripe arrays [63], respectively. Achieving GDY with well-defined structures and distinct properties can make a significant contribution to both fundamental study and development process of such a new type of carbon allotrope. Tailoring the structures of these materials allows readily engineering their mechanical, electronic, and electrochemical properties, leading to numerous striking uses. New GDY-related structures with various morphologies have subsequently emerged, each with novel and unusual properties.

To fulfill the potentially fundamental research and fascinating applications of GDY-based materials, GDY must be available in high quality and large quantity. Several attempts have been reported about establishing feasible pathways for the preparation of GDY over the past decades, such as metal-catalyzed cross-coupling reactions, alkyne metathesis, and templated synthesis. A series of building blocks of GDY have been prepared based on dehydrobenzo[*n*]annulenes [64,65] and perethynylated expanded radialenes [66]. However, such routes mentioned above are not applicable to scalable synthesis of GDY. The high-yield direct scalable preparation of GDY remained a great challenge until Li and co-workers [18] developed an *in-situ* cross-coupling reaction to synthesize large-area ordered thin films of GDY with high quality from hexaethynylbenzene (HEB) precursors on the surface of Cu foils (Figure 6). Copper ions, dissociated from the metallic copper, catalyzed the oxidative homocoupling of HEB. The Cu foils act as not only the catalyst for the cross-

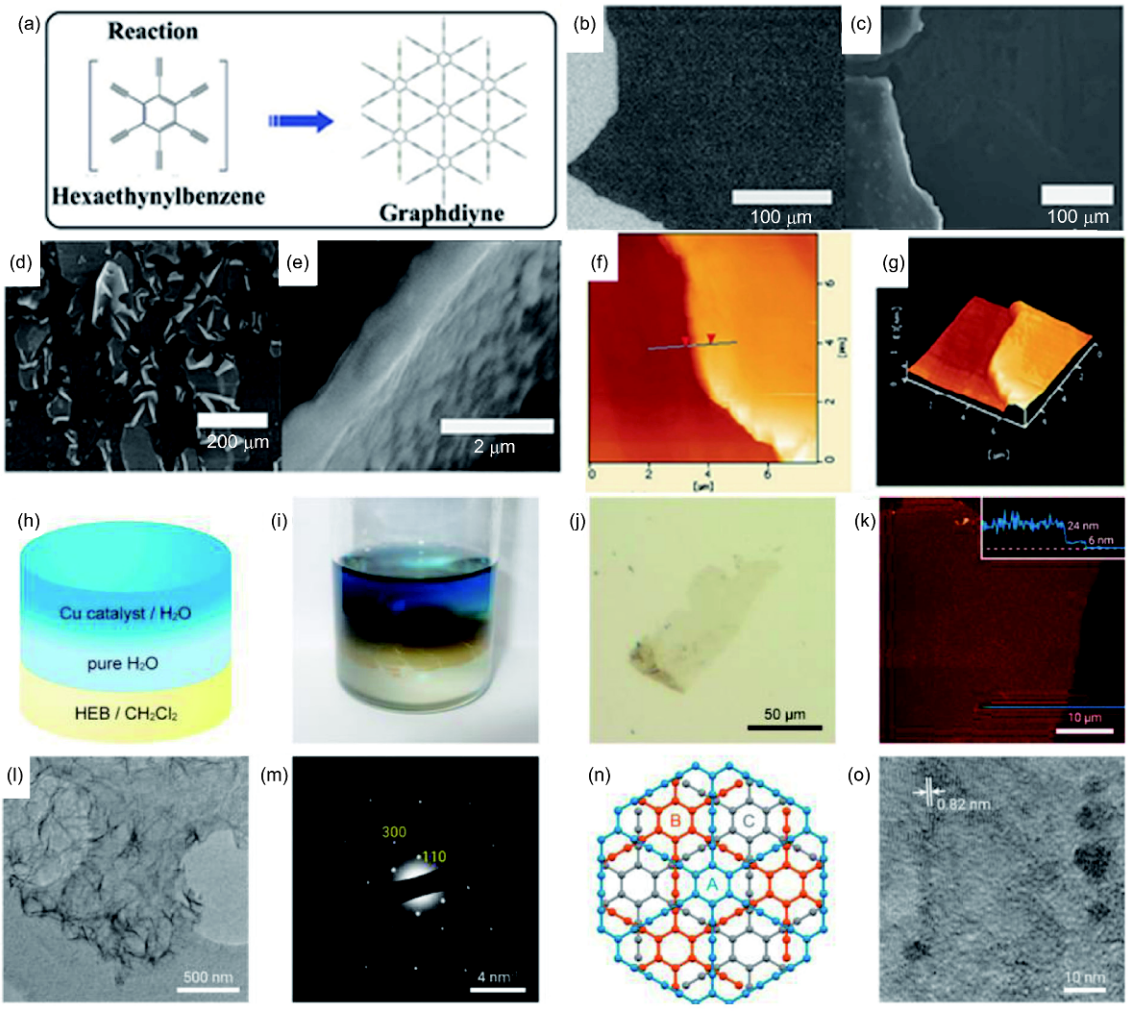

Figure 6 Synthesis and microscopic observations of multilayer GDY. (a) Schematic representation of the synthesis of GDY on Cu foil with hexaethynylbenzene as precursor. SEM images of large-area GDY films grown on the surface of copper foil (b, c), cracked film on the brim of copper foil (d), a turned up film (e). (f) AFM image of GDY film. (g) Tapping-mode 3D height AFM image. Schematic illustration (h) and a photograph (i) of the liquid/liquid interfacial synthetic procedure. (j) Optical microscope image on an HMDS/Si(100) substrate. (k) Atomic force microscope image on HMDS/Si(100) and cross-sectional analysis along the blue line. TEM image (l) and SAED pattern (m) on a holey elastic carbon matrix. Numerical values in panel f denote Miller indices. (n) GDY lattice of the ABC-stacking configuration (top view) determined by TEM/SAED. (o) High-resolution TEM micrograph (color online).

coupling reaction but also the substrate, providing a large and flat space for directional polymerization, for growing the GDY film; accordingly, the polymerization of HEB monomers on the flat Cu surface drives the reaction toward the formation of a diyne-polymer [18]. The conductivity of GDY is calculated to be 2.516×10^{-4} S/m, comparable with that of Si, suggesting the excellent semiconducting properties of GDY. A standard protocol as a primary screen for evaluating the quality of the as-prepared GDY is also established. X-ray photoelectron spectroscopy (XPS), scanning electron microscope (SEM)/EDS, and Raman spectra of the GDY nanosheet showed characteristics consistent with the chemical composition and bonding of GDY. Microscopic analyses, SEM, and atomic force microscopy (AFM) images of GDY film on a copper substrate indicate the uniform of the GDY film. The crystallinity of the GDY nanosheet was confirmed by the transmission electron microscope (TEM) images, the selected area electron diffraction (SAED) pattern, and the X-ray diffraction (XRD, Cu-Kα radiation) pattern. More recently, GDY nanosheet featuring a narrow distributions of thickness (as thin as 3 nm) and lateral size (1.5 μm) was synthesized through a liquid/liquid or gas/liquid interfacial strategy (Figure 6), affording thin and crystalline GDY at room temperature [67]. The electronic structure of GDY exposed to air was investigated by both the X-ray absorption spectroscopy (XAS) and scanning transmission X-ray microscopy [68]. The results confirm the existence of carbon-carbon triple bonds in GDY. Carbon-carbon triple bonds at defect sites in GDY have been observed to change into double bonds after 3 mon of exposure to air. It was also found that most of the functional groups from the aged GDY could be removed after being annealed at high temperature

(e.g., 800 °C) [68].

Carbon nanotubes, as a quintessential nanomaterial, have already compiled an impressive list of superlatives since their discovery in 1991 [7]. The excellent mechanical, unique structural, electrical, thermal and chemical properties of CNTs categorized them as outstanding reinforcement material in nanocomposites [69,70]. Graphyne-based nanotubes were first predicted in 2003 [33]. In 2011, Li's group [60] firstly reported the fabrication of GDY nanotube (GDYNT) arrays using the anodic aluminum oxide template catalyzed by Cu foil. Morphology characterization of GDYNT shows it has a smooth surface with a wall thickness of around 40 nm. After annealing treatment, the wall thickness of the GDYNTs became thin, to about 15 nm, and the length did not change. The morphology-dependent field emission properties of GDY arrays were measured and display high performance field emission properties. The turn-on field and threshold field of GDYNTs annealed decreased to 4.20 and 8.83 V/μm, respectively. Interestingly, GDYNTs exhibited a reduced value of work function and more stability than that of carbon nanotubes. Recent calculations show that zigzag GDYNTs are structurally more stable compared to armchair GDYNTs of the same size [71]. While the bandgaps for both the armchair and zigzag GDYNTs can be tuned as a function of size, the conductivity in each of these two different chiralities is markedly different. Zigzag GDYNTs have wider valence and conduction bands and are expected to have a higher electron- and hole-mobility than their armchair counterparts.

GDY nanowire (GDYNW), a novel aggregate structure of high aspect ratios which shows a very high-quality, defect-free surface, has also been constructed via a vapor-liquid-solid growth process using ZnO nanorod arrays on a silicon slice as the substrate [61]. TEM images reveal that the diameter of a single GDYNW is about 30 to 40 nm with a smooth and uniform surface along the length. The GDYNWs are excellent semiconductors with a conductivity of 1.9×10^3 S/m, which is larger than that of graphdiyne films and most other semiconductors, and comparable to carbon nanotubes and graphene. The GDYNWs also show the average mobility of about 7.1×10^2 $cm^2/V/s$, which is of the same order of magnitude as graphene [72]. These findings suggest that GDYNWs should be a promising and key novel material in electronic and photoelectric fields. More recently, a type of GDY based core/shell architecture nanowires arrays (Cu@GDY NW) has been fabricated with Cu as the core and GDY as the shell [62]. The surface of Cu@GDY NW displays a rippled silk texture, which could effectively supply porous nanostructures with numerous electroactive surface sites. As a model system, it exhibits highly catalytic activity and stability for hydrogen evolution reaction in acidic media. The attractive performances make it a promising candidate for substituting precious catalysts for practical applications.

Compared with other carbon materials [73,74], precise positioning/patterning of GDY is still a challenge for the realization of large-area and flexible organic electronic devices and circuits, mostly due to its intrinsic solution-processed synthesis. As shown in Figure 7, the grooved template provided numerous regularly confined spacing at the microscale for the *in situ* synthesis of GDY, whereas the wettability of grooved templates played a key role in allowing continuous mass transport of raw reactants [63]. After the completion of cross-coupling reaction procedure, precisely patterned graphdiyne stripes can be generated accordingly. The size of graphdiyne stripe arrays is depending on the silicon substrate size (1 cm×1.5 cm), and the layer thickness can be manipulated from just several nanometers to hundreds of nanometers by varying the primary concentration of hexaethynylbenzene monomers. As a proof-of-principle demonstration, a stretchable sensor based on the graphdiyne stripe arrays is performed to monitor the human finger motion. It is expected that this wettability-facilitated strategy will provide new insights into the controlled synthesis of graphdiyne toward promising flexible electronics and other optoelectronic applications.

According to the synthetic route of GDY discussed above, GDY nanowalls were synthesized [75]. By adjusting the ratio of added organic alkali along with the amount of monomer, the proper amount of copper ions was dissolved into the solution, thus forming catalytic reaction sites. With a rapid reaction rate of Glaser-Hay coupling, graphdiyne grew vertically at these sites first, and then with more copper ions dissolved, uniform graphdiyne nanowalls formed on the surface of copper substrate. Raman spectra, UV-vis spectra, and HRTEM results confirmed the features of graphdiyne. These GDY nanowalls also exhibited excellent and stable field-emission properties.

4 Functionalization and applications of GDY-based nanomaterials

Functionalization of pristine GDY, including chemical modification and various covalent/noncovalent interactions with GDY, is one of the best way to strengthen the competitive advantages of GDY in versatile fields. GDY oxide (GDYO), the oxidized form of GDY, can be readily prepared from GDY powder by a modified Hummer's method [76]. The presence of carboxyl groups leads to the reduction of van der Waals interactions between GDY layers, which strongly facilitates the separation of GDY layers into individual ones. Additionally, the attachment of suitable groups renders the GDY soluble in aqueous or organic solvents, opening the possibility of further modifications through subsequent solution-based chemistry. Furthemore,

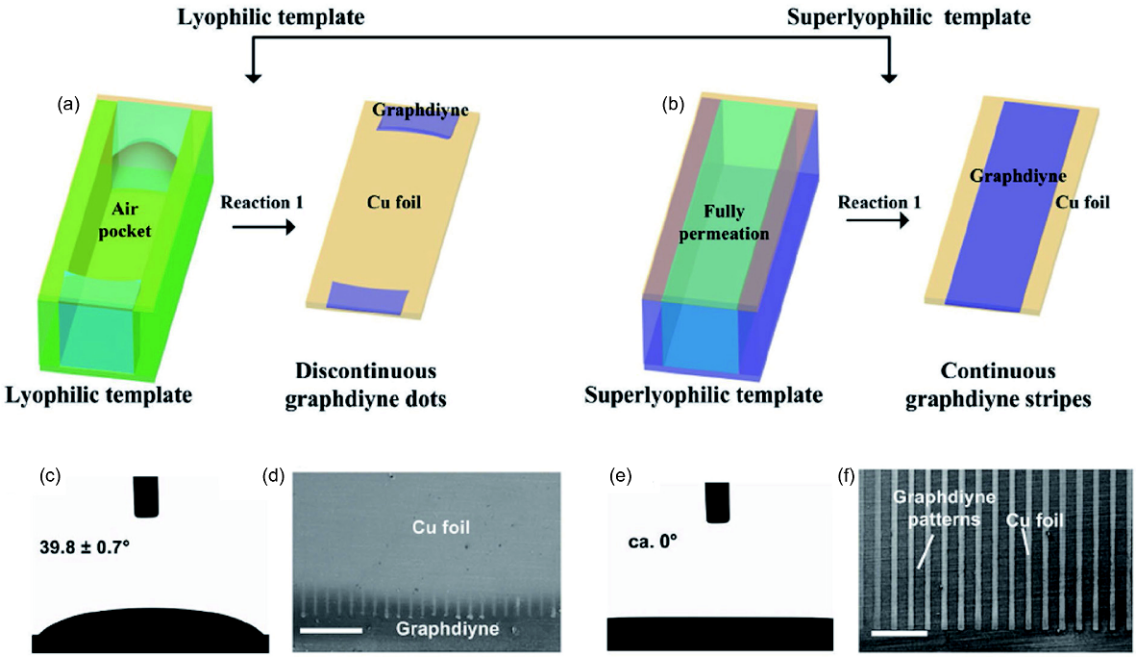

Figure 7 The grooved template provided numerous regularly confined spacing at the microscale for the *in situ* synthesis of GDY, whereas the superlyophilicity of grooved templates is the key to allow a continuous mass transport of raw reactants and yield precisely patterned GDY stripes. (a) When a lyophilic template has been used to guide the growth of graphdiyne, air pockets usually existed in the middle part of the linear confined spacing, yielding just several graphdiyne dots in the two ends of the pillar gap regions. (b) When using a superlyophilic template, the hexaethynylbenzene-loading pyridine liquid can completely wet and pass through the linear confined spacing, allowing the generation of precisely patterned graphdiyne stripes. The contact angles of pyridine (γ=39.82 mN/m) droplet on the lyophilic (c) and superlyophilic (e) grooved templates. (d, f) The corresponding scanning electron microscopic (SEM) images of graphdiyne growth upon the copper foils. The dark areas are graphdiyne while the gray regions are copper foils. The scale bar is 500 μm. Adapted from Ref. [63] (color online).

the GDYO can be used as an even excellent substrate for electroless deposition of ultrafine Pd clusters to form Pd/GDYO nanocomposites, which exhibited a five-fold higher catalytic efficiency when compared with the carbon black counterpart [76]. Recently, as a proof-of-concept demonstration, GDY oxide is used to establish a new platform for fundamental studies on carbon electrochemistry and various electroanalytical applications [77–79]. Doping GDY with heteroatom (e.g., N [80–84], B [84–86], P [87], S [84,88], and F [89]) is an efficient way for the fabrication of various potentially useful GDY-based materials with enhanced performances. For example, isoelectronic doping of GDY with B and N atoms can provide stable configurations with modified band gaps [58]. The electron-donating or electron-withdrawing interaction between heteroatom and carbon atoms induced changes of both atomic charge and spin density [90–92]. In nature, heteroatom doping could induce the delocalization of charge in the GDY plane, and the altered charge distribution in the GDY plane could facilitate the oxygen adsorption and further enhance its electrocatalytic activity. Another alternative way of developing GDY chemistry would be to assemble other analogues with GDY, forming novel nanocomposites with exciting performances. These newly-developed GDY-based materials have been proposed for use in energetic devices.

4.1 Electrochemical catalysis

The rapidly developing of environmentally friendly and renewable energy devices (e.g., fuel cells, batteries, and water splitting) hold great promise for solving current energy and environmental challenges [93–97]. The oxygen reduction reaction (ORR), hydrogen evolution reaction (HER), and oxygen evolution reaction (OER) pose great scientific challenges for the development of efficient catalysts for clean and renewable energy technologies [80,81,98,99]. At present, noble-metal catalysts (e.g. Pt, Ir, Pd) have been regarded as the state-of-the-art electrocatalysts used to promote the ORR in fuel cells for energy conversion, the HER for the generation of hydrogen fuel from the electrochemical splitting of water, and the OER in metal-air batteries for energy storage. But their high-cost, scarcity, poor stability and low abundance limit their practical applications. Therefore, considerable effort have been devoted to develop non-precious electrocatalysts as alternatives to precious ones [100–102]. Among these catalysts, carbon material-based architectures have emerged as interesting candidates due to their tunable molecular structures, abundance and strong tolerance to acid/alkaline environments [101,103–106]. However, the low electrical conductivity and/or limited amount of exposed active sites intrinsically hampered their

practical uses. Therefore, exploring new efficient electrocatalysts with high activity and stability is thus of great demanded. Density functional theory (DFT) calculations revealed that some carbon atoms on GDY have a net positive charge, which can be attributed to the electron transferred from the ring carbon to the nearby sp carbon [31]. These positively charged sites can improve the interaction between GDY and the gases and facilitate the electrocatalytic process. In addition, as a result of the extra alkyne units between the benzene rings in GDY, the pore size of the network is increased to approximately 2.5 Å, which facilitates the adsorption of air into the pores when the sample is exposed to the atmosphere. This are natural advantages of GDY, which should be very beneficial to electrocatalytic process. Therefore, it would be a great advance if GDY-based electrocatalysts can be used as a state-of-the-art electrocatalyst for electrochemical catalysis.

Recently, GDY has been successfully used as the efficient metal-free ORR electrocatalysts [91,92,107,108]. Liu *et al.* [91] demonstrated that the nitrogen-doped GDY could be used as a metal-free electrode with a comparable electrocatalytic activity to commercial Pt/C catalysts for ORR in alkaline fuel cells (Figure 8(a)). In this condition, N-doped GDY shows a better stability and an increased tolerance to the cross-over effect than Pt/C catalysts. Furthermore, dual-heteroatom co-doped GDY was successfully prepared (Figure 8(b)). The rational designed nitrogen and fluorine co-doped GDY was shown to have high selectivity for the four-electron ORR pathway, comparable electrocatalytic activity, and better stability, as well as a higher tolerance to methanol crossover and CO poisoning effects, than commercial Pt/C in alkaline media with great potential for large-scale applications [92]. More recently, the iron-nitrogen co-doped GDY was prepared and exhibited excellent ORR performance following a direct four-electron reduction pathway in both alkaline and acidic electrolytes. Besides, its long-term stability is superior to Pt/C and other GDY-based ORR catalysts [108]. Despite significant advances in developing GDY-based ORR catalysts, developing new GDY-based ORR catalysts with high-performance and long-term stability that can work in acidic electrolyte is still a new direction and challenge.

Similar to ORR, noble metal-based catalysts (e.g. Pt, Pd, RuO_2, and IrO_2) are currently the state-of-the-art for HER and OER, their high cost and scarcity prevent their practical applications. Therefore, the research efforts have focused on the design and fabrication of GDY-based HER and OER catalysts based on transition metals (TMs) [93,96,104,109–112]. Liu *et al.* [91]. In 2016, the first GDY based 3D self-supported Cu@GDY nanowires array (Cu@GDY NA/CF) was developed by our group and was successfully used as an efficient HER electrocatalyst [62]. In 0.5 M H_2SO_4, it exhibits outstanding HER activity and stability superior to most of the reported non-precious HER electrocatalysts. Hybrid coordination derived from GDY and Cu is identified as a highly active molecule catalytic center for HER. Later, GDY nanosheet-supported Co nanoparticles wrapped in N-doped carbon (CoNC/GDY) were prepared and used as HER electrocatalysts at all pH values (Figure 9) [113]. Impressively, CoNC/GDY exhibited outstanding HER activity and unprecedented durability, which could be evidenced by the negligible current change over 36000, 38000, and 9000 cycles under acidic (pH=0), neutral (pH=7.0) and basic (pH=14.0) conditions, respectively—behavior superior to that of commercial Pt/C under respective conditions, which was rarely reported previously.

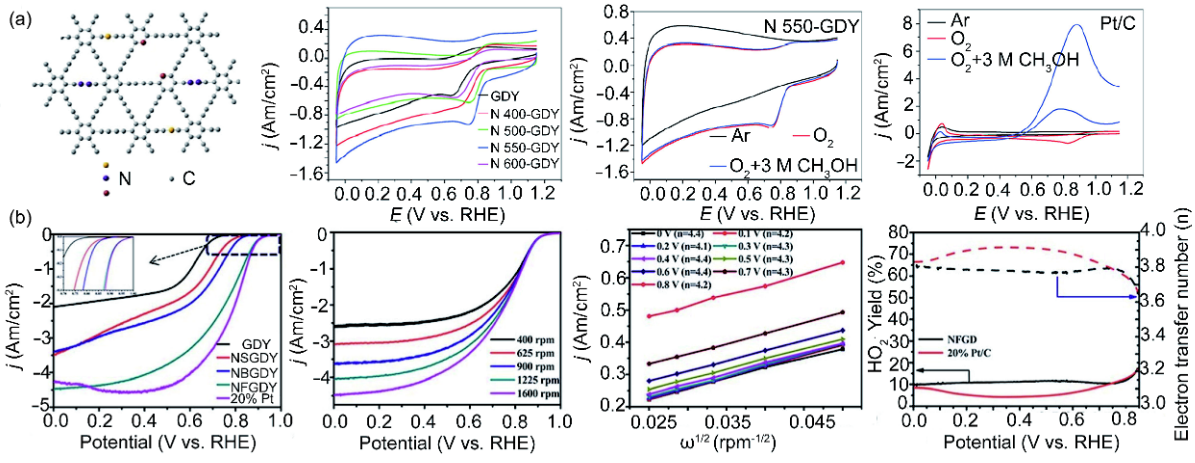

Figure 8 (a) Catalytic performance of N-doped GDY. From left to right: scheme of N-doped GDY; typical CV curves (scan rate 10 mV/s) of GDY and N-doped GDY on a GC RDE in an O_2-saturated 0.1 M KOH solution; CV curves of N 550-GDY and Pt/C in Ar-saturated (black), O_2-saturated (red), 3 M methanol and O_2-saturated 0.1 M KOH (blue) solution. Adapted from Ref. [91]. (b) From left to right: LSV curves of GDY, NSGDY, NBGDY and NFGDY obtained from RDE measurements at 1600 rpm at a scan rate of 10 mV/s in O_2-saturated 0.1 M KOH; LSV curves of NFGDY obtained from RDE measurements at different rotating rates from 400 to 1600 rpm; K–L plots of NFGDY calculated at different potentials on the basis of the RDE data; HO_2^- yields and electron transfer number of NFGD and 20% Pt/C at various disk electrode potentials obtained from the rotating ring-disk electrode tests (color online).

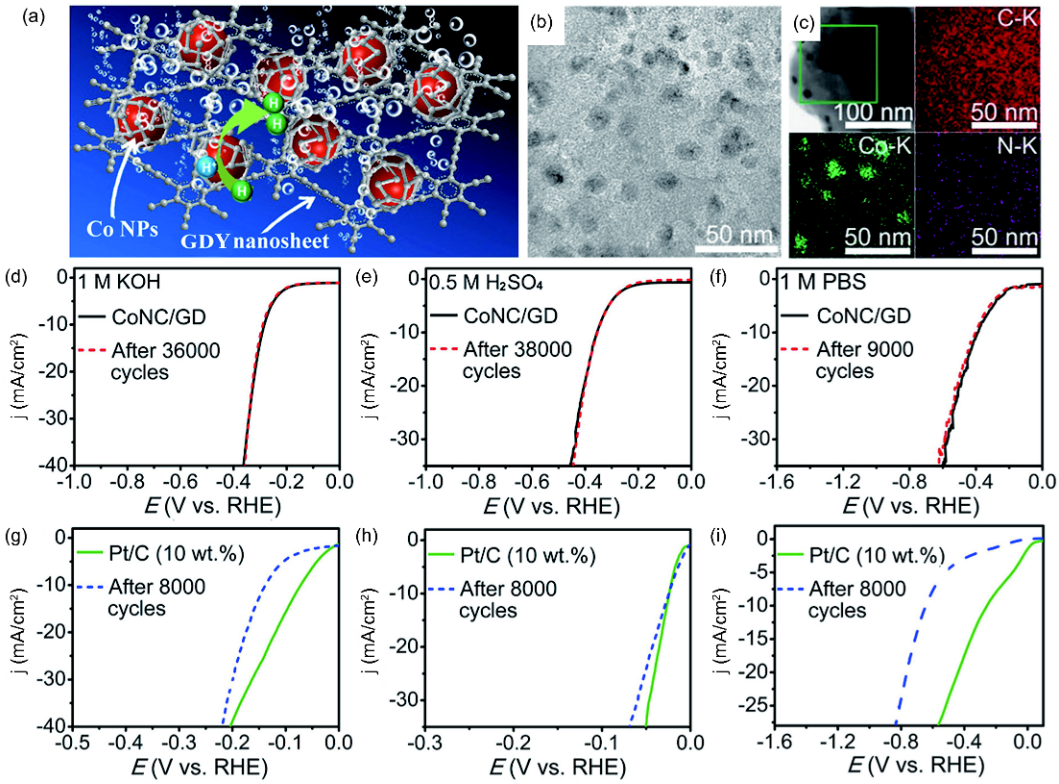

Figure 9 (a) Schematic representation of the CoNC/GDY catalysts. (b) TEM and (c) STEM image and EDX elemental mapping of C, Co, and N for the CoNC/GDY catalyst. HER polarization curves of CoNC/GDY in (d) 1 M KOH initially and after 38000 CV scans (e) 0.5 M H_2SO_4 initially and after 38000 CV scans and (f) 1 M PBS initially and after 9000 CV scans. HER polarization curves of commercial Pt/C (10 wt.%) before and after 8000 CV scans in 1 M KOH (g), 0.5 M H_2SO_4 (h) and 1 M PBS (i). Adapted from Ref. [113] (color online).

To meet the practical applications, the electrocatalysts for OER and HER should be operated in the same conditions, especially in an alkaline electrolyte, based on a single catalyst, to achieve sustained overall water splitting. However, most of the efficient electrocatalysts in acidic conditions may be inactive or even unstable in alkaline conditions, and *vice versa*. The work of Xue *et al.* [114] reported the first GDY supported efficient and bifunctional electrocatalyst, in which 3D GDY foam was used as scaffolds, and $NiCo_2S_4$ nanowires array was used as building blocks ($NiCo_2S_4$ NW/GDF, Figure 10). The resulted electrocatalyst exhibited outstanding catalytic activity and stability toward both OER and HER, as well as overall water splitting in 1.0 M KOH. When used as an alkaline water electrolyzer, it could deliver 10 and 20 mA/cm^2 at low cell voltages of 1.53 and 1.56 V, respectively, and showed excellent stability over 140 h of continuous electrolysis operation at 20 mA/cm^2. Wu and coworkers [115] reported a 3D Cu@GDY/Co electrode with an OER onset potential of ~1.53 V vs. RHE and a potential of 1.65 V vs. RHE to achieve 10 mA/cm^2.

The outstanding electrocatalytic behaviors of these GDY based electrocatalysts could be ascribed from the following reasons. The unique electronic structure and high conductivity of the GDY layers make them highly conductive supporting matrices and facilitate the fast electron transfer in the catalyst. The high porosity of the GDY structure and the well-designed macro/mesoporosity of the electrocatalysts can benefit efficient mass transport and the release of gas bubbles, enabling more efficient use of active sites; the greatly enhanced electrochemically active surface area can maximize the exposure of more active sites. These all lead to significant OER and HER performance improvements. Moreover, the strong associated interactions not only provide more catalytically active sites but also be helpful to the long-term durability of the electrocatalysts.

4.2 Photoelectrochemical (PEC) water splitting

Photoelectrochemical (PEC) hydrogen production from water is another promising approach to producing green chemical fuel because it can integrate the collection and conversion of solar energy into a photoelectrode [93,94,116–119]. Unlike other p-type semiconductors used in the fabrication of photocathodes, such as NiO [120], Cu_2O [121], and p-Si [122], the metal-free GDY has a rigid carbon network with delocalized π-system, natural band gap, remarkable electronic properties, and uniformly distributed pores. Li *et al.* fabricated the first photocathode employing GDY as the

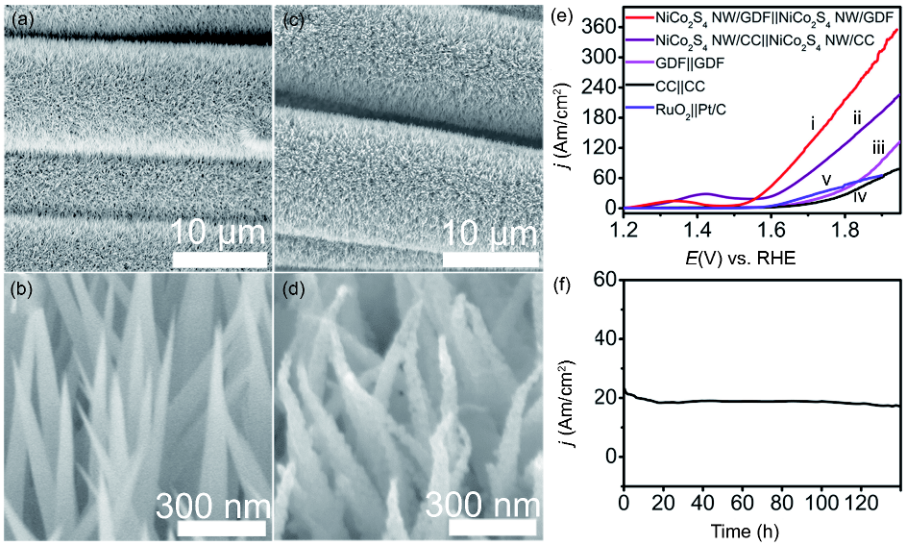

Figure 10 Low- and high-magnification SEM images of (a, b) NiCo-precursor NW/GDF and (c, d) $NiCo_2S_4$ NW/GDF. (e) Two electrode OER polarization curves (without iR compensation) of $NiCo_2S_4$ NW/GDF||$NiCo_2S_4$ NW/GDF, $NiCo_2S_4$ NW/CC||$NiCo_2S_4$ NW/CC, GDF||GDF, CC||CC, and RuO_2||Pt/C. (f) Two-electrode cell stability of $NiCo_2S_4$ NW/GDF||$NiCo_2S_4$ NW/GDF electrode in 1.0 M KOH (color online).

hole transfer layer into a PEC water splitting cell (Figure 11) [123]. The existence of relatively strong π-π interactions between GDY and mercaptopyridine surface-functionalized CdSe quantum dots (CdSe QDs) facilitates the hole transportation and photocurrent enhancement. These results are attributed to the higher hole mobility and stability of GDY. In another study [124], a composite GDY/$BiVO_4$ photoanode was fabricated by direct synthesis of GDY nanowalls on a $BiVO_4$ electrode. A considerable enhancement of the photoelectrochemical behavior of $BiVO_4$ was observed after the GDY coating.

4.3 Photocatalysis

The increasing demand in the development of novel hybrid materials for effective photocatalysis motivated the researchers to utilize the recently emerged 2D carbon allotropes toward advancements in semiconductor photocatalysis. The diacetylenic linkage of GDY can transform in part into a 2D π-conjugated structure favorable for electronic transmission after hydrothermal treatments, thereby enabling its use as an electron-transport material in photodegradation processes. Interestingly, the graphdiyne-ZnO nanohybrids showed superior photocatalytic properties on the degradation of two azo dyes (methylene blue and rhodamine B) than that of the bare ZnO nanoparticles [125]. The rate constant of graphdiyne-ZnO nano-hybrids is nearly 2-fold higher compared to that of the bare ZnO nanoparticles on the photodegradation of both azo dyes. Moreover, GDY can improve the photocatalytic performance of TiO_2 due to its large surface area and high electron mobility. Accordingly, the GDY-TiO_2 nanocomposites (P25-GDY) were prepared and used as photocatalyst in the degradation of methylene blue (MB), showing a significantly higher activity than the bare P25, P25-CNTs, and P25-graphene under both UV and visible light irradiation [126]. The complicated charge transfer behaviors between GDY and anatase TiO_2 of different crystal facets was further investigated [127]. The results of first-principles DFT show that the TiO_2(001)-GDY composite exhibits the most outstanding performance in rich electronic structure, charge separation, and the oxidation ability compared with pure TiO_2(001) or TiO_2(001)-graphene composite, which makes it an excellent photocatalyst candidate with high efficiency. In the photocatalytic degradation of methylene blue (MB), the rate constant when using the TiO_2(001)-GDY composite was 1.63 times that of the pure TiO_2(001) and 1.27 times that of the TiO_2(001)-graphene composite. Therefore, the TiO_2(001)-GDY composite was recognized as an excellent candidate for use as a high-efficiency photocatalyst.

4.4 Photodetectors

Ultraviolet (UV) thin-film photodetectors have wide applications in commercial and military areas due to their virtues of structural simplicity, low-cost fabrication, and room-temperature operation. Many efforts have been done to improve the sensitivity of ZnO thin film photodetectors. Jin *et al.* [128] synthesized GDY:ZnO nanocomposites by self-assembly of GDY nanoparticles onto the surface of *n*-propylamine-modified ZnO NPs, and were then used to fabricate UV photo-detectors. They found that the device exhibits high responsivity of 1260 A/W and short rise/decay time of 6.1/2.1 s. In comparison, the conventional reference device

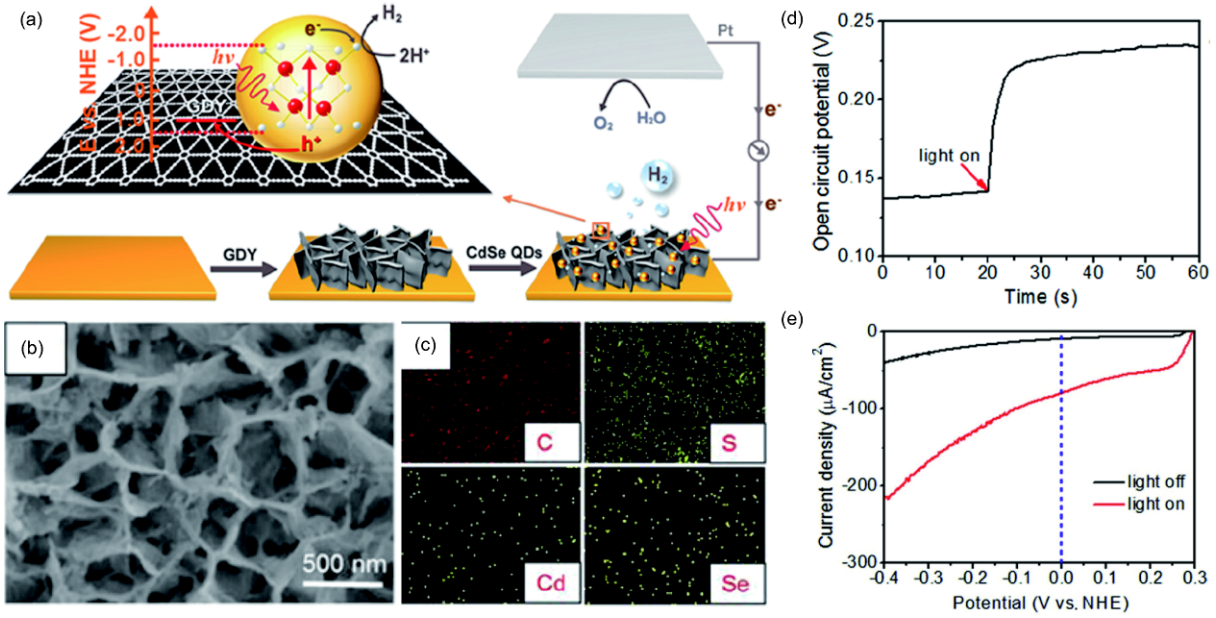

Figure 11 (a) Schematic diagram of the PEC cell, consisting of the assembled CdSe QDs/GDY photocathode, Pt wire as counter electrode, and corresponding interfacial migration process of the photogenerated excitons. (b) SEM images of the assembled CdSe QDs/GDY film. (c) The elemental mapping of carbon, selenium, sulfur and cadmium. (d) Open circuit potential response of the CdSe QDs/GDY photocathode under dark and illuminated conditions (300 W Xe lamp). (e) LSV scanning from 0.3 to −0.4 V at 2 mV/s with light off (black trace) and on (red trace) [123] (color online).

owns a much lower R of 174 A/W and much longer rise/decay time of 32.1/28.7 s. Their experimental results suggest that the junction formed between the GDY NP and ZnO NP greatly improves the carrier-exchange process between the two NPs, and hence significantly enhances the photoresponse.

4.5 Supercapacitors

Electrochemical capacitors, also called supercapacitors (SCs), which can store energy using either ion adsorption (electrochemical double layer capacitors) or fast surface redox reactions (pseudo-capacitors), have attracted a great deal of attention owing to their high power density, better cycling lifespan, fast charging and discharging, environmental benignity relative to the conventional electric capacitors [129–131]. A notable improvement in performance has been achieved through recent advances in understanding charge storage mechanisms and the development of advanced nanostructured materials. The discovery that ion desolvation occurs in pores smaller than the solvated ions has led to higher capacitance for electrochemical double layer capacitors using carbon electrodes with subnanometre pores, and opened the door to designing high-energy density devices using a variety of electrolytes. Krishnamoorthy *et al.* [132] investigated the GDY nanostructures based supercapacitor by cyclic voltammetry and charge-discharge analysis. Cyclic-voltammetric studies exhibited quasi-rectangular profiles, indicating the presence of EDLCs and Faradaic capacitance. At a constant discharge current density 3.5 A/g, the GDY electrodes delivered a specific capacitance of 71.4 F/g. The specific capacitance is higher than other carbon materials such as graphene and graphene oxide [133,134]. The cyclic stability tests demonstrated excellent capacitance retention of about 97% after 1000 cycles, which measured by cycle voltammetric method. These excellent electrochemical properties could be ascribed to its special structural characterizations (sp and sp^2-co-hybridized carbons, highly π-conjugated structure, uniformly distributed pores and natural bandgap). The structure of GDY with uniformly distributed pores makes them promising candidates for adsorption/desorption and facilitates diffusion of electrolyte ions both in-plane and out-plane directions. Recent studies showed that N-doped GDY [135] and GDY nanowalls [136] could also be used for highly specific capacitances and cyclic stabilities. The studies demonstrated GDY electrodes offer a great potential toward application on supercapacitors.

4.6 Lithium-ion capacitors

Lithium-ion capacitors (LICs) are hybrid energy storage devices containing a conventional high-energy lithium-ion battery (LIB) electrode combined with a high-power capacitor electrode [137]. However, the usage of traditional LICs, which consist of an activated carbon cathode (positive electrodes) and a carbonaceous lithium-intercalating anode (negative electrode), is mainly limited by their relatively low

energy storage capacity [138–140]. Recently, based on first-principles calculations, Zhang *et al.* [141] reported that the atomic arrangement of GDY leads to a unique Li triangular occupation pattern, i.e., each pore accommodates three Li atoms located at three symmetric sites. Li can easily penetrate GDY plane with an energy barrier of 0.35 eV, which enables Li atoms to be well dispersed on both sides of single-layer GDY. The maximum Li storage capacity of GDY monolayers can be as high as LiC_3 with triangular-patterned Li atoms distributing alternately on both sides of GDY, which is twice the capacity of graphite and multilayered GDY. The work of Jang *et al.* [142] demonstrated that the composite of the Li-intercalated multilayer α-GDY was $C_6Li_{7.31}$ and that the calculated voltage was suitable for the anode. The practical specific/volumetric capacities of α-GDY (2719 mA h/g, 2032 mA h/cm^3) are much greater than that of graphite (~372 mA h/g~818 mA h/cm^3), graphynes (~1117 mA h/g~1589 mA h/cm^3), and γ-GDY (~744 mA h/g), respectively. Our calculations suggest that multilayer a-graphdiyne can serve as a promising high-capacity lithium ion battery anode. Therefore, GDY appears to be a promising high-capacity anode material for Li-ion batteries. As reported by Du *et al.* [143], LIC comprised of GDY anode and an activated carbon (AC) cathode delivered an initial specific energy as high as 112.2 W h/kg at a power density of 400.1 W/kg, with 94.7% retention after 1000 cycles. Even at a power density of 1000.4 W/kg, it delivered an energy density of 95.1 W h/kg, operated in the voltage range of 2−4 V (Figure 12). Those high energy and power density associated with GDY has a highly porous nanostructure and high specific surface area, resulting in further increase the electrolyte-material contact area and short transport pathways for electrons and ions. GDY exhibited excellent electrochemical performance, suggesting its promising application as an efficient electrode for next generation batteries.

4.7 Lithium-ion batteries

Lithium-ion batteries (LIBs) is considered to be the most promising energy storage technology in portable electronics devices and electrical vehicles due to its high energy and power density, high safety, and good cycling stability. Graphite is regarded as the commercialized anodes because of its good lifespan and high coulombic efficiency, but limited by low storage capacity of 372 mA h/g [144]. Novel electrode materials with excellent high-rate capability and ultralong life cycle, which is the key step toward enabling LIB integration, are therefore highly desirable [145]. Theoretical results demonstrated that the practical specific/volumetric capacities of GDY (2719 mA h/g for α-GDY, 744 mA h/g for γ-GDY) is much greater than the values of graphite (372 mA h/g) [142]. The energetics and dynamics of Li in GDY monolayers demonstrated that GDY enabled both in-plane and out-plane diffusion of Li ions with moderate barriers (0.35–0.52 eV), suggesting GDY can serve as a promising Lithium-ion batteries anode [141].

Inspired by this, efforts have been made in the preparation of GDY based electrodes and their applications as anodes. Huang *et al.* [146] reported the application of GDY in lithium storage materials and expounding the method of lithium storage in multilayer GDY (Figure 13). It is found that the battery reversible capacity reaches as high as 520 mA h/g after 400 cycles at a current density of 500 mA/g. Even at a high current density of 2 A/g, the cells still retained their high specific capacity at 420 mA h/g after 1000 cycles.

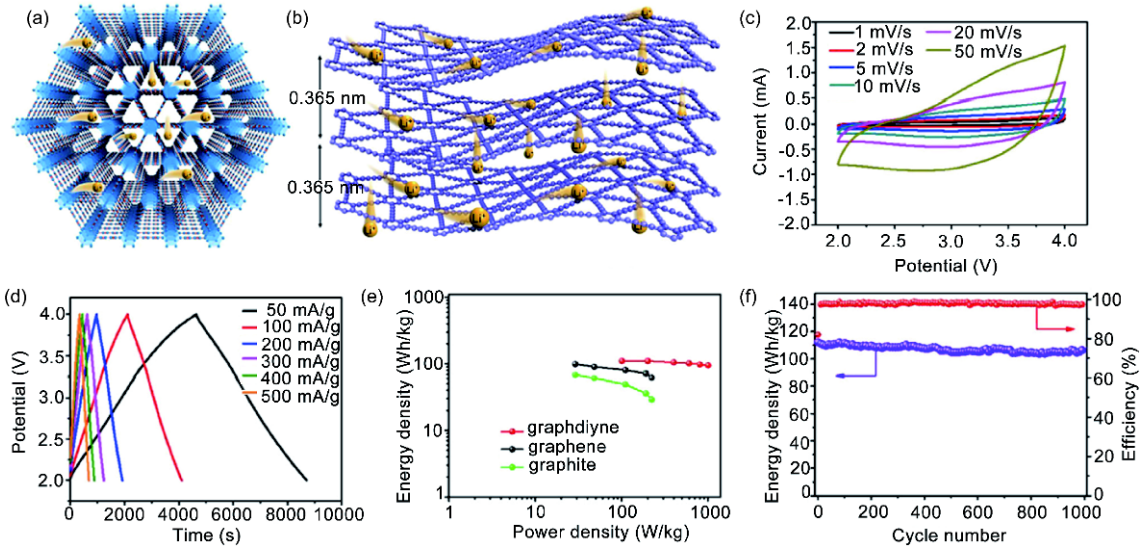

Figure 12 Lithium diffusion in GDY layers top view (a), side view (b). (c) CV curves at various scan rates. (d) Galvanostatic charge-discharge voltage profiles at various current densities. (e) Ragone plots of GDY/AC LICs compared with previously reported graphite and graphene LICs. (f) Cycling stability of GDY/AC LIC at a current density of 200 mA/g [143] (color online).

Moreover, The Li atom storage in multilayer GDY could be occurred in two ways as inter-layer insertion/extraction and surface absorption/desorption process. The inter-layer insertion/extraction method of Li storage in multi-layer GDY corresponded to a Li storage capacity of LiC_6. Li and coworkers [147] presented the scalable preparation of high-quality GDY nanotubes and ultrathin GDY nanosheets and their applications as anodes. It was reported that such nanostructures exhibited a high capacity of 1388 mA h/g and high rate performance (870 mA h/g at 10 A/g, and 449.8 mA h/g at 20 A/g) with robust stability, demonstrating outstanding overall potential for its applications.

Recent studies demonstrated that heteroatom-doping is an efficient way for improving the electrochemical performance of bulk GDY materials [148–151]. For example, the N-doped GDY electrode showed reversible capacity as high as 785 mA h/g after 200 cycles at a current density of 0.2 A/g, while the GDY electrode was 584 mA h/g [149]. Chlorine-substituted GDY (Cl-GDY) film, as an anode material in practical LIBs, could reach a highly reversible capacity of 1150 mA h/g at 50 mA/g and a stable specific capacity around 500 mA h/g for 500 cycles at the current density as higher as 2 A/g in lithium-ion half-cells [151]. More recently, hydrogen substituted GDY was prepared and used as carbon-rich flexible electrode for lithium and sodium ion batteries, showing large reversible capacities of 1050 mA h/g for lithium ion batteries and 650 mA h/g for sodium ion batteries [150].

4.8 Na-ion batteries

Na-ion batteries (NIBs) have been considered as promising candidates for large-scale electricity storage mainly due to their low cost and the natural abundance of Na resource [152,153]. The larger atomic radii of Na and lower kinetics of Na^+ insertion/extraction are the major challenge in the replacement of Li with Na [154]. Based on the Grimme DFT-D2 method, Niaei *et al.* [155] determined the maximum capacity, energy barriers for Na diffusion throughout the layers, and expansion of the layers due to Na insertion. Their

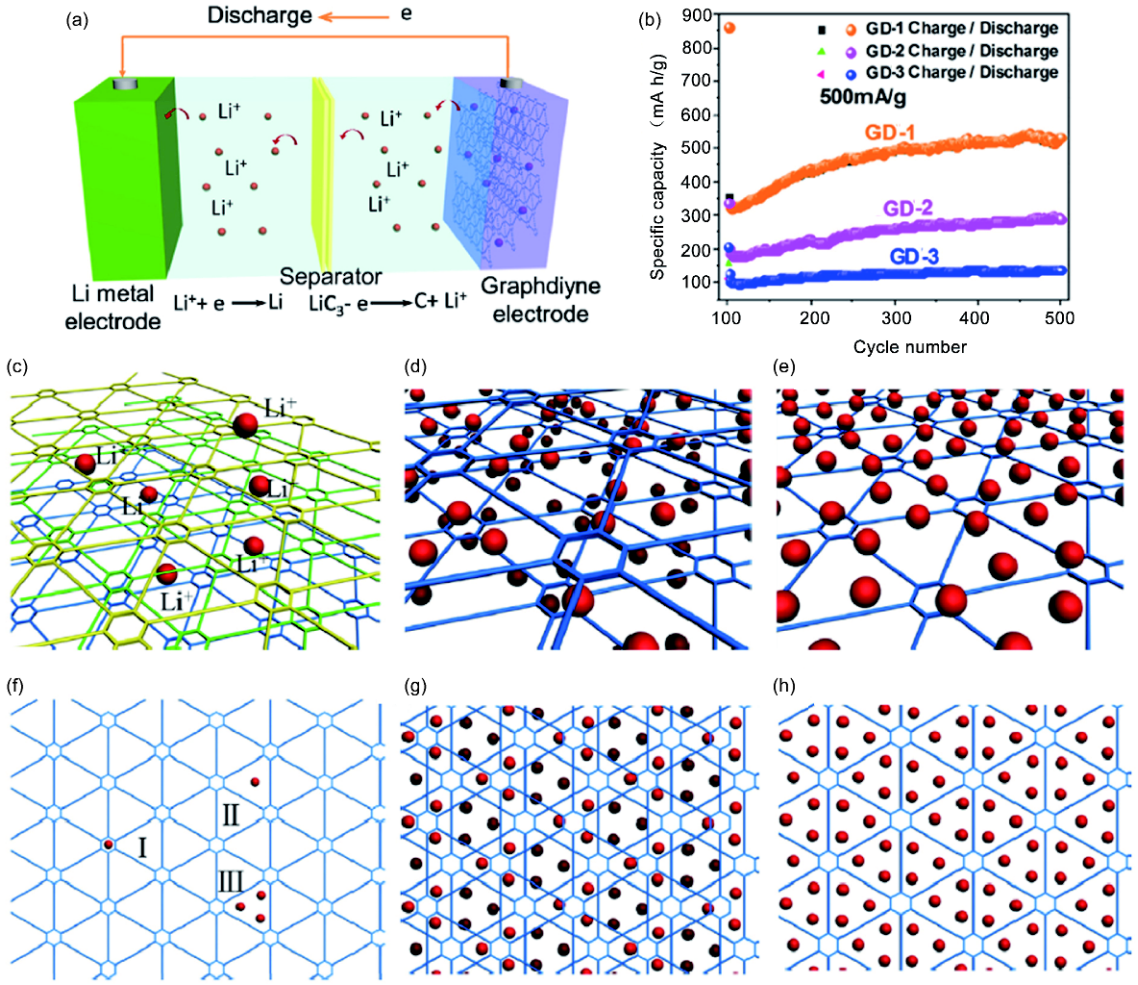

Figure 13 (a) Schematic representation of an assembled GDY-based battery. (b) Cycle performance of the GDY-1, GDY-2, and GDY-3 electrodes at a current density of 500 mA/g between 5 mV and 3 V. Li-storage of GDY in a Li-ion cell: (c) Li-intercalated GDY. (d) Three different sites for occupation by Li atoms in GDY, absorption of Li atoms on (e, f) both sides and (g, h) one side of a GDY plane [146] (color online).

results indicate that Na intercalates within the GDY bulk layers with a capacity of $NaC_{5.14}$ without expansion (316 mA h/g) and $NaC_{2.57}$ with expansion of 28% (497 mA h/g). The energy barrier for movement of Na in the slit pore formed by two GDY bulk layers is found to be 0.82 eV for bulk GDY with an AB-2 stacking, and the barrier for movement through a GDY sheet is found to be 0.12 eV. The barrier for movement in the slit pore formed by sheets becomes even lower for AB-3 stacking, with values of 0.68 and 0.40 eV found for different pathways. Movement from one GDY sheet to another for the AB-3 stacking also has a moderate energy of 0.37 eV. Zhang *et al.* [156] explored its sodium storage properties, which exhibited a reversible capacity of 261 mA h/g after 300 cycles at a current density of 50 mA/g. Even at a high current density of 100 mA/g, the as-prepared GDY electrodes delivered a moderate specific capacity of 211 mA h/g after 1000 cycles, with excellent capacity retention of 98.2% (Figure 14). By theoretical calculations associated with experimental research, the GDY electrodes assembled sodium ion batteries have shown extraordinary electrochemical performance, including excellent rate performance, long cycle life and moderate specific capacity. GDY have been recognized as a promising anode material in Na-ion batteries.

4.9 Solar cells

Perovskite solar cells (PSCs) have drawn dramatically increased attentions as one of the most promising candidates for solar energy harvesting, due to their high power conversion efficiencies (PCE), low cost and easy fabrication [157–159]. GDY has been successfully introduced into perovskite solar cells as a dopant into poly(3-hexylthiophene) (P3HT) working as hole-transporting material (HTM) for effective hole transport [160,161]. Due to high charge transport capability of GDY and the formation of efficient percolation paths in the active layer, the introduction of GDY can effectively improve the short circuit current (J_{sc}) and power conversion efficiency (PCE) of the polymer solar cells [160]. On the other hand, some GDY aggregates exhibit a scattering nature, and thus help to increase the light absorption of the perovskite solar cells in the long wavelength range. As high as 14.58% light-to-electricity conversion efficiency was achieved, superior to the pristine P3HT-based devices [161]. Recently, GDY was doped into PCBM layer of perovskite solar cell with an inverted structure (ITO/PEDOT:PSS/$CH_3NH_3PbI_{3-x}Cl_x$/PCBM:GDY/C_{60}/Al) to improve the electron transport [162]. As reported, the optimized power conversion efficiency (PCE) of 14.8% was achieved. In comparison with pure PCBM-based devices, an average PCE of PCBM:GDY-based devices was observed with 28.7% enhancement (13.9% vs. 10.8%). Detailed studies revealed that the introduction of GDY into PCBM film could improve the electrical conductivity, electron mobility, and charge extraction, which also benefit to the enhancement of J_{sc} and FF. Ren *et al.* [163] found that dye-sensitized solar cells (DSSCs) using platinum nanoparticles modified GDY nanosheet (PtNP-GDYNS) as the counter electrode had

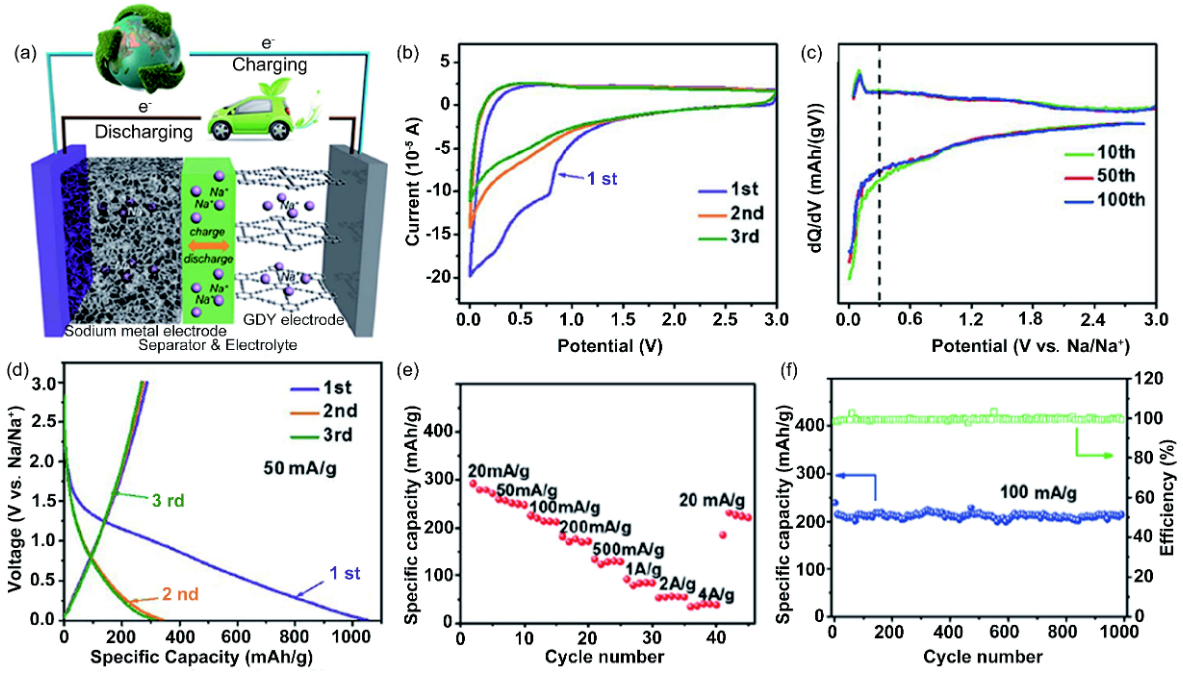

Figure 14 (a) Schematic of a sodium ion battery based on GDY. (b) Cyclic voltammogram (CV) profiles of the GDY-based electrode at a scan rate of 0.2 mV/s. (c) Differential curves of charge/discharge profiles of the GDY-based electrode at a current density of 50 mA/g. (d) Galvanostatic charge-discharge profiles at a current density of 50 mA/g for the first three cycles. (e) Rate performance at varied current density ranging from 20 to 4000 mA/g. (f) Cycle performance at a current density of 100 mA/g [156] (color online).

improved performance compared to that of precious Pt foil and better than that of Pt nanoparticles and rGO/Pt nanoparticle composites (Figure 15), which could be ascribed to their special "p-n" junction-like structure with improved catalytic activity and excellent electron transfer ability [163]. The power conversion efficiency of DSSCs that use PtNP-GDYNS (6.35%) counter electrode has been significant improved compared to using the conventional PtNP (5.39%) and PtNP-reduced graphene oxide (5.94%), indicating that the reaction of I_3^-/I^- redox pairs is greatly catalyzed by using PtNP-GDYNS as the counter electrode. This may open up a new route to GDY nanocomposites that serve as high-performance counter electrodes for photoelectric conversions.

Colloidal quantum dot (CQD) photovoltaics can combine facile solution processability with quantum-size-effect tunability to match absorption with the solar spectrum [164,165]. Jin *et al.* [166] employed GDY as anode buffer layer in colloidal quantum dots solar cells. Compared to relevant reference devices, power conversion efficiency is notably enhanced from 9.49% to 10.64%. It is found that the hole transfer from the quantum dot solid active layer to the anode can be enhanced by the introduction of GDY, which can effectively reduce the work function of the colloidal quantum dot solid. They also found that the all-carbon buffer layer reducing surface recombination on the back side of the photovoltaic device to delay the carrier lifetime. Therefore, the introduction of GDY into solar cell applications will become a simple and effective strategy for improving device performances in the future.

5 Conclusions and perspectives

Since its first synthesis in large-scale by Li and co-workers in 2010, GDY has come a long way. Several detailed reviews [2,16,28,99,167–170] and books [171] have been devoted to this topic. There have been significantly advancements in synthetic techniques, which can now produce reasonably GDY, from multi-films to monolayers. New GDY-related structures with various morphologies (e.g., GDY nanosheets, GDY nanotubes, GDY nanowires, GDY stripes, and GDY nanowalls) have subsequently emerged, each with novel and unusual properties. Tailoring the structures of these materials allows readily engineering their mechanical, electronic, and electrochemical properties, leading to numerous striking uses. However, developing and optimizing processing methods to create well-defined GDY-based nanostructures are still in their infancy. Achieving GDY and GDY-based nanostructures with different well-defined structures and distinct properties may make a significant contribution to both fundamental study and development process of such a new type of carbon allotrope.

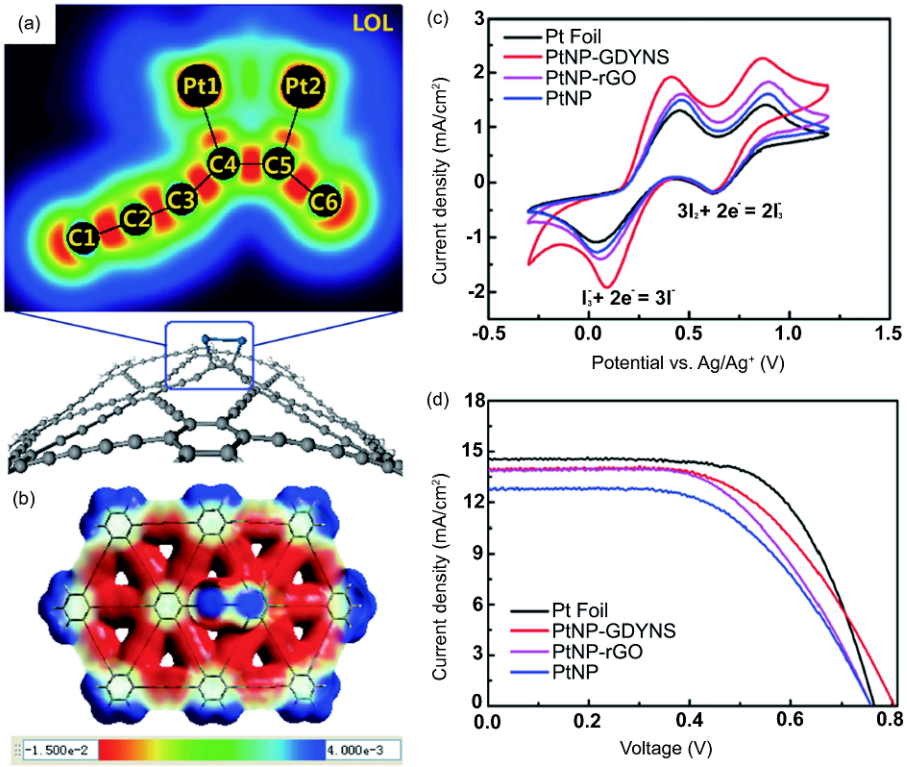

Figure 15 (a) Localized orbital locator (LOL) maps and Mayer bond order analysis for the Pt_2-GDY fragment (off-center adsorption site). (b) ESP surfaces with an isovalue of 0.0004 e/au^3 for Pt_2-GDY (off-center adsorption site). (c) Cyclic voltammetry curves of different counter electrodes. (d) Photocurrent density-voltage (*J-V*) curves of DSSCs using different counter electrodes [163] (color online).

GDY-based materials have shown considerable potential applications in energetic fields (electrochemical catalysis, photocatalysis, photovoltaics, Li batteries, and solar cells, etc.), but application-orientated research is only just beginning. Nowadays, researchers in the world believe that many bottlenecks of current renewable and clean energy devices can be broken by using GDY. With biggest advances in understanding the catalytic nature of these GDY-based materials by means of both theoretical simulations and experimental characterizations, and combining this with the development of appropriate preparation technology, we believe that materials based on GDY have a bright future.

Acknowledgements This work was supported by the National Natural Science Foundation of China (21790050**,** 21790051), the National Key Research and Development Project of China (2016YFA0200104) and the Key Program of the Chinese Academy of Sciences (QYZDY-SSW-SLH015).

Conflict of interest The authors declare that they have no conflict of interest.

1 Heimann RB, Evsvukov SE, Koga Y. *Carbon*, 1997, 35: 1654–1658
2 Li Y, Xu L, Liu H, Li Y. *Chem Soc Rev*, 2014, 43: 2572–2586
3 Georgakilas V, Perman JA, Tucek J, Zboril R. *Chem Rev*, 2015, 115: 4744–4822
4 Li Y. *Sci Sin Chim*, 2017, 47: 1045–1056
5 Jia Z, Li Y, Zuo Z, Liu H, Huang C, Li Y. *Acc Chem Res*, 2017, 50: 2470–2478
6 Kroto HW, Heath JR, O'Brien SC, Curl RF, Smalley RE. *Nature*, 1985, 318: 162–163
7 Iijima S. *Nature*, 1991, 354: 56–58
8 Novoselov KS, Geim AK, Morozov SV, Jiang D, Zhang Y, Dubonos SV, Grigorieva IV, Firsov AA. *Science*, 2004, 306: 666–669
9 Baughman RH, Eckhardt H, Kertesz M. *J Chem Phys*, 1987, 87: 6687–6699
10 Boehm HP, Setton R, Stumpp E. *Carbon*, 1986, 24: 241–245
11 Narita N, Nagai S, Suzuki S, Nakao K. *Phys Rev B*, 1998, 58: 11009–11014
12 Haley MM, Brand SC, Pak JJ. *Angew Chem Int Ed Engl*, 1997, 36: 836–838
13 Diederich F. *Nature*, 1994, 369: 199–207
14 Bunz UHF, Rubin Y, Tobe Y. *Chem Soc Rev*, 1999, 28: 107–119
15 Wan WB, Brand SC, Pak JJ, Haley MM. *Chem-Eur J*, 2000, 6: 2044–2052
16 Huang CS, Li YL. *Acta Phys-Chim Sin*, 2016, 32: 1314–1329
17 Wan WB, Haley MM. *J Org Chem*, 2001, 66: 3893–3901
18 Li G, Li Y, Liu H, Guo Y, Li Y, Zhu D. *Chem Commun*, 2010, 46: 3256–3258
19 Long M, Tang L, Wang D, Li Y, Shuai Z. *ACS Nano*, 2011, 5: 2593–2600
20 He J, Ma SY, Zhou P, Zhang CX, He C, Sun LZ. *J Phys Chem C*, 2012, 116: 26313–26321
21 Cranford SW, Brommer DB, Buehler MJ. *Nanoscale*, 2012, 4: 7797–7809
22 Puigdollers AR, Alonso G, Gamallo P. *Carbon*, 2016, 96: 879–887
23 Ma SY, Zhang M, Sun LZ, Zhang KW. *Carbon*, 2016, 99: 547–555
24 Chopra S. *RSC Adv*, 2016, 6: 89934–89939
25 Inagaki M, Kang FY. *J Phys Chem A*, 2014, 2: 13193–13206
26 Zheng JJ, Zhao X, Zhao Y, Gao X. *Sci Rep*, 2013, 3: 1271
27 Tahara K, Yamamoto Y, Gross DE, Kozuma H, Arikuma Y, Ohta K, Koizumi Y, Gao Y, Shimizu Y, Seki S, Kamada K, Moore JS, Tobe Y. *Chem Eur J*, 2013, 19: 11251–11260
28 Ivanovskii AL. *Prog Solid State Chem*, 2013, 41: 1–19
29 Chandra Shekar S, Swathi RS. *J Phys Chem A*, 2013, 117: 8632–8641
30 Yue Q, Chang S, Tan J, Qin S, Kang J, Li J. *Phys Rev B*, 2012, 86: 235448
31 Srinivasu K, Ghosh SK. *J Phys Chem C*, 2012, 116: 5951–5956
32 Pan LD, Zhang LZ, Song BQ, Du SX, Gao HJ. *Appl Phys Lett*, 2011, 98: 173102
33 Coluci VR, Braga SF, Legoas SB, Galvão DS, Baughman RH. *Phys Rev B*, 2003, 68: 035430
34 Cranford SW, Buehler MJ. *Carbon*, 2011, 49: 4111–4121
35 Bai H, Zhu Y, Qiao W, Huang Y. *RSC Adv*, 2011, 1: 768–775
36 Tang Y, Yang H, Yang P. *Carbon*, 2017, 117: 246–251
37 Hou J, Yin Z, Zhang Y, Chang T. *J Appl Mech*, 2015, 82: 094501
38 Yang Y, Xu X. *Comput Mater Sci*, 2012, 61: 83–88
39 Yue Q, Chang S, Kang J, Qin S, Li J. *J Phys Chem C*, 2013, 117: 14804–14811
40 Kang J, Li J, Wu F, Li SS, Xia JB. *J Phys Chem C*, 2011, 115: 20466–20470
41 Kresse G, Hafner J. *Phys Rev B*, 1993, 47: 558–561
42 Zhang YY, Pei QX, Wang CM. *Appl Phys Lett*, 2012, 101: 081909
43 Luo G, Qian X, Liu H, Qin R, Zhou J, Li L, Gao Z, Wang E, Mei WN, Lu J, Li Y, Nagase S. *Phys Rev B*, 2011, 84: 075439
44 Jiao Y, Du A, Hankel M, Zhu Z, Rudolph V, Smith SC. *Chem Commun*, 2011, 47: 11843–11845
45 Pei Y. *Physica B-Condensed Matter*, 2012, 407: 4436–4439
46 Sun L, Jiang PH, Liu HJ, Fan DD, Liang JH, Wei J, Cheng L, Zhang J, Shi J. *Carbon*, 2015, 90: 255–259
47 Cui HJ, Sheng XL, Yan QB, Zheng QR, Su G. *Phys Chem Chem Phys*, 2013, 15: 8179–8185
48 Zheng Q, Luo G, Liu Q, Quhe R, Zheng J, Tang K, Gao Z, Nagase S, Lu J. *Nanoscale*, 2012, 4: 3990–3996
49 Luo G, Zheng Q, Mei WN, Lu J, Nagase S. *J Phys Chem C*, 2013, 117: 13072–13079
50 Leenaerts O, Partoens B, Peeters FM. *Appl Phys Lett*, 2013, 103: 013105
51 Wang XM, Lu SS. *J Phys Chem C*, 2013, 117: 19740–19745
52 Bhattacharya B, Singh NB, Mondal R, Sarkar U. *Phys Chem Chem Phys*, 2015, 17: 19325–19341
53 Shohany BG, Roknabadi MR, Kompany A. *Physica E*, 2016, 84: 146–151
54 Zhu Y, Bai H, Huang Y. *Chemistryopen*, 2016, 5: 78–87
55 Cirera B, Zhang YQ, Björk J, Klyatskaya S, Chen Z, Ruben M, Barth JV, Klappenberger F. *Nano Lett*, 2014, 14: 1891–1897
56 Owens FJ. *Solid State Commun*, 2017, 250: 75–78
57 Li C, Li J, Wu F, Li SS, Xia JB, Wang LW. *J Phys Chem C*, 2011, 115: 23221–23225
58 Bu H, Zhao M, Zhang H, Wang X, Xi Y, Wang Z. *J Phys Chem A*, 2012, 116: 3934–3939
59 Mohajeri A, Shahsavar A. *J Mater Sci*, 2017, 52: 5366–5379
60 Li G, Li Y, Qian X, Liu H, Lin H, Chen N, Li Y. *J Phys Chem C*, 2011, 115: 2611–2615
61 Qian X, Ning Z, Li Y, Liu H, Ouyang C, Chen Q, Li Y. *Dalton Trans*, 2012, 41: 730–733
62 Xue Y, Guo Y, Yi Y, Li Y, Liu H, Li D, Yang W, Li Y. *Nano Energy*, 2016, 30: 858–866
63 Wang SS, Liu HB, Kan XN, Wang L, Chen YH, Su B, Li YL, Jiang L. *Small*, 2017, 13: 1602265
64 Youngs WJ, Tessier CA, Bradshaw JD. *Chem Rev*, 1999, 99: 3153–3180
65 Spitler EL, Johnson CA, Haley MM. *Chem Rev*, 2006, 106: 5344–5386
66 Gholami M, Tykwinski RR. *Chem Rev*, 2006, 106: 4997–5027
67 Matsuoka R, Sakamoto R, Hoshiko K, Sasaki S, Masunaga H, Nagashio K, Nishihara H. *J Am Chem Soc*, 2017, 139: 3145–3152

68 Zhong J, Wang J, Zhou JG, Mao BH, Liu CH, Liu HB, Li YL, Sham TK, Sun XH, Wang SD. *J Phys Chem C*, 2013, 117: 5931–5936
69 Iijima S, Ichihashi T. *Nature*, 1993, 363: 603–605
70 Ajayan PM. *Chem Rev*, 1999, 99: 1787–1800
71 Pari S, Cuéllar A, Wong BM. *J Phys Chem C*, 2016, 120: 18871–18877
72 Burghard M, Klauk H, Kern K. *Adv Mater*, 2009, 21: 2586–2600
73 Zhou X, Boey F, Zhang H. *Chem Soc Rev*, 2011, 40: 5221–5231
74 Park S, Pitner G, Giri G, Koo JH, Park J, Kim K, Wang H, Sinclair R, Wong HSP, Bao Z. *Adv Mater*, 2015, 27: 2656–2662
75 Zhou J, Gao X, Liu R, Xie Z, Yang J, Zhang S, Zhang G, Liu H, Li Y, Zhang J, Liu Z. *J Am Chem Soc*, 2015, 137: 7596–7599
76 Qi H, Yu P, Wang Y, Han G, Liu H, Yi Y, Li Y, Mao L. *J Am Chem Soc*, 2015, 137: 5260–5263
77 Guo S, Yan H, Wu F, Zhao L, Yu P, Liu H, Li Y, Mao L. *Anal Chem*, 2017, 89: 13008–13015
78 Zhuang X, Mao L, Li Y. *Electrochem Commun*, 2017, 83: 96–101
79 Wang C, Yu P, Guo S, Mao L, Liu H, Li Y. *Chem Commun*, 2016, 52: 5629–5632
80 Gong K, Du F, Xia Z, Durstock M, Dai L. *Science*, 2009, 323: 760–764
81 Liang HW, Zhuang X, Brüller S, Feng X, Müllen K. *Nat Commun*, 2014, 5: 4973
82 Guo D, Shibuya R, Akiba C, Saji S, Kondo T, Nakamura J. *Science*, 2016, 351: 361–365
83 Liu X, Dai L. *Nat Rev Mater*, 2016, 1: 16064
84 Liu Y, Shen Y, Sun L, Li J, Liu C, Ren W, Li F, Gao L, Chen J, Liu F, Sun Y, Tang N, Cheng HM, Du Y. *Nat Commun*, 2016, 7: 10921
85 Wang S, Iyyamperumal E, Roy A, Xue Y, Yu D, Dai L. *Angew Chem Int Ed*, 2011, 50: 11756–11760
86 Yang L, Jiang S, Zhao Y, Zhu L, Chen S, Wang X, Wu Q, Ma J, Ma Y, Hu Z. *Angew Chem Int Ed*, 2011, 50: 7132–7135
87 Zhang Y, Mori T, Ye J, Antonietti M. *J Am Chem Soc*, 2010, 132: 6294–6295
88 Yang Z, Yao Z, Li G, Fang G, Nie H, Liu Z, Zhou X, Chen X', Huang S. *ACS Nano*, 2012, 6: 205–211
89 Sun X, Zhang Y, Song P, Pan J, Zhuang L, Xu W, Xing W. *ACS Catal*, 2013, 3: 1726–1729
90 Wu P, Du P, Zhang H, Cai C. *J Phys Chem C*, 2012, 116: 20472–20479
91 Liu R, Liu H, Li Y, Yi Y, Shang X, Zhang S, Yu X, Zhang S, Cao H, Zhang G. *Nanoscale*, 2014, 6: 11336–11343
92 Zhang S, Cai Y, He H, Zhang Y, Liu R, Cao H, Wang M, Liu J, Zhang G, Li Y, Liu H, Li B. *J Mater Chem A*, 2016, 4: 4738–4744
93 Walter MG, Warren EL, McKone JR, Boettcher SW, Mi Q, Santori EA, Lewis NS. *Chem Rev*, 2010, 110: 6446–6473
94 Chen X, Shen S, Guo L, Mao SS. *Chem Rev*, 2010, 110: 6503–6570
95 Pham TA, Ping Y, Galli G. *Nat Mater*, 2017, 16: 401–408
96 Turner JA. *Science*, 2004, 305: 972–974
97 Lubitz W, Ogata H, Rüdiger O, Reijerse E. *Chem Rev*, 2014, 114: 4081–4148
98 Magasinski A, Dixon P, Hertzberg B, Kvit A, Ayala J, Yushin G. *Nat Mater*, 2010, 9: 353–358
99 Deng D, Novoselov KS, Fu Q, Zheng N, Tian Z, Bao X. *Nat Nanotech*, 2016, 11: 218–230
100 Li H, Tsai C, Koh AL, Cai L, Contryman AW, Fragapane AH, Zhao J, Han HS, Manoharan HC, Abild-Pedersen F, Nørskov JK, Zheng X. *Nat Mater*, 2016, 15: 48–53
101 Jaramillo TF, Jørgensen KP, Bonde J, Nielsen JH, Horch S, Chorkendorff I. *Science*, 2007, 317: 100–102
102 Chen Y, Yu G, Chen W, Liu Y, Li GD, Zhu P, Tao Q, Li Q, Liu J, Shen X, Li H, Huang X, Wang D, Asefa T, Zou X. *J Am Chem Soc*, 2017, 139: 12370–12373
103 Kibsgaard J, Chen Z, Reinecke BN, Jaramillo TF. *Nat Mater*, 2012, 11: 963–969
104 Kibsgaard J, Jaramillo TF, Besenbacher F. *Nat Chem*, 2014, 6: 248–253
105 Geng X, Sun W, Wu W, Chen B, Al-Hilo A, Benamara M, Zhu H, Watanabe F, Cui J, Chen TP. *Nat Commun*, 2016, 7: 10672
106 Yin Y, Han J, Zhang Y, Zhang X, Xu P, Yuan Q, Samad L, Wang X, Wang Y, Zhang Z, Zhang P, Cao X, Song B, Jin S. *J Am Chem Soc*, 2016, 138: 7965–7972
107 Lv Q, Si W, Yang Z, Wang N, Tu Z, Yi Y, Huang C, Jiang L, Zhang M, He J, Long Y. *ACS Appl Mater Interfaces*, 2017, 9: 29744–29752
108 Li Y, Guo C, Li J, Liao W, Li Z, Zhang J, Chen C. *Carbon*, 2017, 119: 201–210
109 McCrory CCL, Jung S, Peters JC, Jaramillo TF. *J Am Chem Soc*, 2013, 135: 16977–16987
110 McCrory CCL, Jung S, Ferrer IM, Chatman SM, Peters JC, Jaramillo TF. *J Am Chem Soc*, 2015, 137: 4347–4357
111 Cabán-Acevedo M, Stone ML, Schmidt JR, Thomas JG, Ding Q, Chang HC, Tsai ML, He JH, Jin S. *Nat Mater*, 2015, 14: 1245–1251
112 Wang Q, Hisatomi T, Jia Q, Tokudome H, Zhong M, Wang C, Pan Z, Takata T, Nakabayashi M, Shibata N, Li Y, Sharp ID, Kudo A, Yamada T, Domen K. *Nat Mater*, 2016, 15: 611–615
113 Xue Y, Li J, Xue Z, Li Y, Liu H, Li D, Yang W, Li Y. *ACS Appl Mater Interfaces*, 2016, 8: 31083–31091
114 Xue Y, Zuo Z, Li Y, Liu H, Li Y. *Small*, 2017, 13: 1700936
115 Li J, Gao X, Jiang X, Li XB, Liu Z, Zhang J, Tung CH, Wu LZ. *ACS Catal*, 2017, 7: 5209–5213
116 Gray HB. *Nat Chem*, 2009, 1: 7–7
117 Berardi S, Drouet S, Francàs L, Gimbert-Suriñach C, Guttentag M, Richmond C, Stoll T, Llobet A. *Chem Soc Rev*, 2014, 43: 7501–7519
118 Ran J, Zhang J, Yu J, Jaroniec M, Qiao SZ. *Chem Soc Rev*, 2014, 43: 7787–7812
119 Wu LZ, Chen B, Li ZJ, Tung CH. *Acc Chem Res*, 2014, 47: 2177–2185
120 Li F, Fan K, Xu B, Gabrielsson E, Daniel Q, Li L, Sun L. *J Am Chem Soc*, 2015, 137: 9153–9159
121 Paracchino A, Laporte V, Sivula K, Grätzel M, Thimsen E. *Nat Mater*, 2011, 10: 456–461
122 Ding Q, Zhai J, Cabán-Acevedo M, Shearer MJ, Li L, Chang HC, Tsai ML, Ma D, Zhang X, Hamers RJ, He JH, Jin S. *Adv Mater*, 2015, 27: 6511–6518
123 Li J, Gao X, Liu B, Feng Q, Li XB, Huang MY, Liu Z, Zhang J, Tung CH, Wu LZ. *J Am Chem Soc*, 2016, 138: 3954–3957
124 Gao X, Li J, Du R, Zhou J, Huang MY, Liu R, Li J, Xie Z, Wu LZ, Liu Z, Zhang J. *Adv Mater*, 2017, 29: 1605308
125 Thangavel S, Krishnamoorthy K, Krishnaswamy V, Raju N, Kim SJ, Venugopal G. *J Phys Chem C*, 2015, 119: 22057–22065
126 Wang S, Yi L, Halpert JE, Lai X, Liu Y, Cao H, Yu R, Wang D, Li Y. *Small*, 2012, 8: 265–271
127 Yang N, Liu Y, Wen H, Tang Z, Zhao H, Li Y, Wang D. *ACS Nano*, 2013, 7: 1504–1512
128 Jin Z, Zhou Q, Chen Y, Mao P, Li H, Liu H, Wang J, Li Y. *Adv Mater*, 2016, 28: 3697–3702
129 Yuan C, Li J, Hou L, Zhang X, Shen L, Lou XWD. *Adv Funct Mater*, 2012, 22: 4592–4597
130 Chen Z, Qin Y, Weng D, Xiao Q, Peng Y, Wang X, Li H, Wei F, Lu Y. *Adv Funct Mater*, 2009, 19: 3420–3426
131 Liu J, Jiang J, Cheng C, Li H, Zhang J, Gong H, Fan HJ. *Adv Mater*, 2011, 23: 2076–2081
132 Krishnamoorthy K, Thangavel S, Chelora Veetil J, Raju N, Venugopal G, Kim SJ. *Int J Hydrogen Energy*, 2016, 41: 1672–1678
133 Chen CM, Zhang Q, Yang MG, Huang CH, Yang YG, Wang MZ. *Carbon*, 2012, 50: 3572–3584
134 Ramachandran R, Saranya M, Velmurugan V, Raghupathy BPC, Jeong SK, Grace AN. *Appl Energy*, 2015, 153: 22–31
135 Shang H, Zuo Z, Zheng H, Li K, Tu Z, Yi Y, Liu H, Li Y, Li Y. *Nano Energy*, 2018, 44: 144–154
136 Wang K, Wang N, He J, Yang Z, Shen X, Huang C. *Electrochim Acta*, 2017, 253: 506–516
137 Park MS, Lim YG, Kim JH, Kim YJ, Cho J, Kim JS. *Adv Energy Mater*, 2011, 1: 1002–1006

138 Wang H, Zhang Y, Ang H, Zhang Y, Tan HT, Zhang Y, Guo Y, Franklin JB, Wu XL, Srinivasan M, Fan HJ, Yan Q. *Adv Funct Mater*, 2016, 26: 3082–3093
139 Ding J, Wang H, Li Z, Cui K, Karpuzov D, Tan X, Kohandehghan A, Mitlin D. *Energy Environ Sci*, 2015, 8: 941–955
140 Lee JH, Shin WH, Ryou MH, Jin JK, Kim J, Choi JW. *ChemSusChem*, 2012, 5: 2328–2333
141 Zhang H, Xia Y, Bu H, Wang X, Zhang M, Luo Y, Zhao M. *J Appl Phys*, 2013, 113: 044309
142 Jang B, Koo J, Park M, Lee H, Nam J, Kwon Y, Lee H. *Appl Phys Lett*, 2013, 103: 263904
143 Du H, Yang H, Huang C, He J, Liu H, Li Y. *Nano Energy*, 2016, 22: 615–622
144 Jiang T, Bu F, Feng X, Shakir I, Hao G, Xu Y. *ACS Nano*, 2017, 11: 5140–5147
145 Zheng Y, Zhou T, Zhao X, Pang WK, Gao H, Li S, Zhou Z, Liu H, Guo Z. *Adv Mater*, 2017, 29: 1700396
146 Huang C, Zhang S, Liu H, Li Y, Cui G, Li Y. *Nano Energy*, 2015, 11: 481–489
147 Shang H, Zuo Z, Li L, Wang F, Liu H, Li Y, Li Y. *Angew Chem Int Ed*, 2018, 57: 774–778
148 Zhang S, Liu H, Huang C, Cui G, Li Y. *Chem Commun*, 2015, 51: 1834–1837
149 Zhang S, Du H, He J, Huang C, Liu H, Cui G, Li Y. *ACS Appl Mater Interfaces*, 2016, 8: 8467–8473
150 He J, Wang N, Cui Z, Du H, Fu L, Huang C, Yang Z, Shen X, Yi Y, Tu Z, Li Y. *Nat Commun*, 2017, 8: 1172
151 Wang N, He J, Tu Z, Yang Z, Zhao F, Li X, Huang C, Wang K, Jiu T, Yi Y, Li Y. *Angew Chem Int Ed*, 2017, 56: 10740–10745
152 Kundu D, Talaie E, Duffort V, Nazar LF. *Angew Chem Int Ed*, 2015, 54: 3431–3448
153 Pan H, Hu YS, Chen L. *Energy Environ Sci*, 2013, 6: 2338
154 Qian J, Chen Y, Wu L, Cao Y, Ai X, Yang H. *Chem Commun*, 2012, 48: 7070–7072
155 Farokh Niaei AH, Hussain T, Hankel M, Searles DJ. *J Power Sources*, 2017, 343: 354–363
156 Zhang S, He J, Zheng J, Huang C, Lv Q, Wang K, Wang N, Lan Z. *J Mater Chem A*, 2017, 5: 2045–2051
157 Liu M, Johnston MB, Snaith HJ. *Nature*, 2013, 501: 395–398
158 Eperon GE, Burlakov VM, Docampo P, Goriely A, Snaith HJ. *Adv Funct Mater*, 2014, 24: 151–157
159 Cao J, Liu YM, Jing X, Yin J, Li J, Xu B, Tan YZ, Zheng N. *J Am Chem Soc*, 2015, 137: 10914–10917
160 Du H, Deng Z, Lü Z, Yin Y, Yu LL, Wu H, Chen Z, Zou Y, Wang Y, Liu H, Li Y. *Synth Met*, 2011, 161: 2055–2057
161 Xiao J, Shi J, Liu H, Xu Y, Lv S, Luo Y, Li D, Meng Q, Li Y. *Adv Energy Mater*, 2015, 5: 1401943
162 Kuang C, Tang G, Jiu T, Yang H, Liu H, Li B, Luo W, Li X, Zhang W, Lu F, Fang J, Li Y. *Nano Lett*, 2015, 15: 2756–2762
163 Ren H, Shao H, Zhang L, Guo D, Jin Q, Yu R, Wang L, Li Y, Wang Y, Zhao H, Wang D. *Adv Energy Mater*, 2015, 5: 1500296
164 Emin S, Singh SP, Han L, Satoh N, Islam A. *Sol Energy*, 2011, 85: 1264–1282
165 Carey GH, Abdelhady AL, Ning Z, Thon SM, Bakr OM, Sargent EH. *Chem Rev*, 2015, 115: 12732–12763
166 Jin Z, Yuan M, Li H, Yang H, Zhou Q, Liu H, Lan X, Liu M, Wang J, Sargent EH, Li Y. *Adv Funct Mater*, 2016, 26: 5284–5289
167 Chen Y, Liu H, Li Y. *Chin Sci Bull*, 2016, 61: 2901–2912
168 Li YJ, Li YL. *Acta Phys-Chim Sin*, 2018, 34: 992–1013
169 Zhou JY, Zhang J, Liu ZF. *Acta Phys-Chim Sin*, 2018, 34: 977–991
170 Zhao YS, Zhang LJ, Qi J, Jin Q, Lin KF, Wang D. *Acta Phys-Chim Sin*, 2018, 34: 1048–1060
171 Xu R, Xu Y. *Modern Inorganic Synthetic Chemistry*, 2nd ed. Amsterdam: Elsevier, 2017